

# Lawrence Berkeley National Laboratory

## Recent Work

### Title

CURVED WAVEFRONT CORRECTIONS FOR PHOTOELECTRON SCATTERING

### Permalink

<https://escholarship.org/uc/item/746881n4>

### Authors

Barton, J.J.  
Shirley, D.A.

### Publication Date

1985-03-01



# Lawrence Berkeley Laboratory

UNIVERSITY OF CALIFORNIA

## Materials & Molecular Research Division

Submitted to The Physical Review, B

CURVED WAVEFRONT CORRECTIONS FOR  
PHOTOELECTRON SCATTERING

J.J. Barton and D.A. Shirley

March 1985

RECEIVED  
LAWRENCE  
BERKELEY LABORATORY

APR 25 1985

LIBRARY AND  
DOCUMENTS SECTION

**TWO-WEEK LOAN COPY**  
*This is a Library Circulating Copy  
which may be borrowed for two weeks.*



LBL-18692  
c.2

## **DISCLAIMER**

This document was prepared as an account of work sponsored by the United States Government. While this document is believed to contain correct information, neither the United States Government nor any agency thereof, nor the Regents of the University of California, nor any of their employees, makes any warranty, express or implied, or assumes any legal responsibility for the accuracy, completeness, or usefulness of any information, apparatus, product, or process disclosed, or represents that its use would not infringe privately owned rights. Reference herein to any specific commercial product, process, or service by its trade name, trademark, manufacturer, or otherwise, does not necessarily constitute or imply its endorsement, recommendation, or favoring by the United States Government or any agency thereof, or the Regents of the University of California. The views and opinions of authors expressed herein do not necessarily state or reflect those of the United States Government or any agency thereof or the Regents of the University of California.

CURVED WAVEFRONT CORRECTIONS FOR PHOTOELECTRON SCATTERING

J.J. Barton and D.A. Shirley

Materials and Molecular Research Division  
Lawrence Berkeley Laboratory

and

Department of Chemistry  
University of California  
Berkeley, California 94720

ABSTRACT

We derive new, simplified formulas for the scattering of  $l=1$  spherical waves from central potentials, as a basis for discussing curved wavefront corrections to single-scattering plane-wave models for Angle-Resolved Photoemission Extended Fine Structure (ARPEFS) and Extended X-ray Absorption Fine Structure (EXAFS). A differential form for the expansion of the screened spherical wave replaces the usual Gaunt integral form to facilitate the summation over equivalent magnetic sublevels in the scattered wave. Spherical wave scattering factors are defined and interpreted as corrections to the plane-wave scattering factor. We argue and demonstrate by example that the remarkable success of plane-wave models does not result from reaching the spherical wave asymptotic limit; instead successive partial wave corrections cancel for backscattering at high energy. The new scattering formulas allow curved-wavefront numerical calculations to be performed with little more effort than plane-wave formulas.

## I. INTRODUCTION

Understanding the motion of unbound electrons in solids is an interesting problem with important implications for surface structure determination methods based on electron scattering. The energy range from 20-200 eV has been studied extensively as a basis for the analysis of Low Energy Electron Diffraction (LEED) data;<sup>1-3</sup> more recent work in the energy range 20-1000 eV has been inspired by the explosive growth in the number of Extended X-ray Absorption Fine Structure (EXAFS) measurements.<sup>4</sup> In the case of LEED, the incident electron plane wave is simply described, but it excites every atom in the surface region, leading to a complex scattering problem; in the case of EXAFS only a single chemical element is excited by the x-ray beam, but the entire x-ray absorption process must be understood and the observed modulations correspond to a special multiple scattering event.<sup>5</sup> Thus we suggest that an even more recent technique,<sup>6</sup> Angle-Resolved Photoemission Extended Fine Structure (ARPEFS) may be a more straightforward measurement for further understanding of electron scattering in the 50-1000 eV range. ARPEFS measures partial cross-section oscillations of photoelectrons: only electrons from a single chemical element are measured and a  $4\pi$  angular integration is not necessary. This paper investigates one aspect of the theory of electron scattering in solids, the role of curved wave corrections to the plane-wave single-scattering of (1s) photoelectrons.

A more practical motivation for this work is the interesting discrepancy between ARPEFS measurements and simple scattering theory results for the c(2x2)S/Ni(100) system. Experimentally, a relatively simple Fourier transform spectrum led to the conclusion that only

nearest neighbor and backscattering non-neighboring atoms contributed substantially to the observed spectrum.<sup>6</sup> In other words, the number of important scattering atoms was small, permitting a simple interpretation of the Fourier spectrum. This conclusion has been recently challenged by Bullock, Fadley, and Orders<sup>7</sup> on the basis of single-scattering, plane-wave theoretical calculations. They demonstrated that a great many ion-cores should contribute to the theoretical curve under these and certain other approximations and hence no simple assignment of the Fourier peaks should be possible. Unfortunately, the reproduction of the experimental oscillations by these theoretical calculations is very poor, and we are led to question the conclusions drawn from them.

To settle this issue, an improved theoretical calculation capable of matching the measured curves within experimental accuracy seems in order; if we know that the sum of the calculated scattering events is correct, then we can compare the relative intensity of these events with more confidence. The plane-wave single-scattering calculations may be improved by:

- i) a more accurate atomic-like photoemission wavefunction (unscattered, direct wave),
- ii) curved wave corrections,
- iii) multiple scattering,
- iv) improved elastic scattering phase shifts, and
- v) more accurate inelastic damping.

These improvements are somewhat entwined, but in this paper we will concentrate on a single issue: when are curved wave (also called spherical wave) corrections important?

We will examine only the simplest case of spherical wave scattering: single scattering of photoelectrons excited from a (1s) core level. We derive new formulas for this scattering in section II, applicable to both ARPEFS and EXAFS experiments. These formulas facilitate a qualitative discussion of curved wave corrections which occupies section III. In section IV we evaluate individual terms in these formulae for the example of a Ni atom potential. Our discussion in section V centers on possible generalizations to higher angular momenta. Finally, we address the impact our results might have on calculation of extended fine structure.

## II. CURVED WAVE SCATTERING OF $l=1$ PHOTOELECTRONS

Our scattering system consists of a photoemitting atom and an array of non-overlapping ion-core potentials. Zero-order calculation of the photoemission partial cross-section would ignore the ion-core array and only consider the atomic-like photoabsorption. Corrections caused by scattering from the ion core potentials gives the ARPEFS oscillations. Since we are only concerned with the oscillations, the details of zero-order calculation are not relevant: we need only know the zero-order wave function. With dipole selection rules, polarized light, a (1s) core-level initial state, and complete metallic screening the zero-order wave function is proportional to:

$$\psi_0(\vec{r}) = ih_1(kr)Y_{10}(\hat{r}) \quad (1)$$

Here  $h_l(kr)$  is the spherical Hankel function of the first kind<sup>8</sup> (we will omit the usual superscript (1) as in  $h_l^{(1)}(kr)$  and we will not use

spherical Hankel functions of the second kind),  $Y_{\ell m}(\hat{r})$  is the spherical harmonic evaluated at the angles given by the unit vector,  $\hat{r}$ , in the direction of  $\vec{r}$ , and  $k$  is the electron's wavenumber far from the photoemitter. Notice that we have selected the polarization vector of the light for our  $\hat{z}$  axis to simplify the zero-order wave function description. The first-order corrections to this wave function are generated by including scattered waves emanating from each nearby ion core. The partial wave method<sup>9</sup> for calculating these scattered waves has three steps:

- i) expand the incident wave as an angular momentum series about the ion-core position,
- ii) multiply each "partial wave" in this series by a (complex) scattering amplitude (which also shifts the wave phase),
- iii) sum the non-zero partial waves to give the full scattered wave.

It is the first step which distinguishes plane wave from spherical wave scattering.

#### A. PLANE WAVES

As a basis for our discussion of the curved wave effects we repeat the derivation of the plane wave ARPEFS model first presented by Lee,<sup>5</sup> but following more closely the method used by Lee and Pendry<sup>10</sup> in their derivation of the EXAFS formula.

In a plane wave approximation,<sup>5</sup> the photoelectron wave is represented near the scattering center by the value of the wave at the center, times a plane wave:



$$\psi_0(\vec{r}) = ih_1(kr) \left(\frac{3}{4\pi}\right)^{1/2} \cos \theta_{\epsilon a} e^{ika \cdot (\vec{r} - \vec{a})} \quad (2)$$

where  $\theta_{\epsilon a}$  is the angle between the electric vector  $\hat{\epsilon}$  and the bond vector  $\vec{a}$ . Since we have already ignored wavefront curvature with this approximation, we replace the Hankel function by its asymptotic limit,

$$i^l h_l(ka) \sim \frac{e^{ika}}{ika} \quad (3)$$

and apply the well-known Bauer formula,

$$e^{i\vec{k} \cdot \vec{r}} = \sum_{l=0}^{\infty} (2l+1) i^l j_l(kr) P_l(\cos \theta_{kr}) \quad (4)$$

to expand the photoelectron wave around the scattering center:

$$\psi_0(\vec{r}) = \left(\frac{3}{4\pi}\right)^{1/2} \cos \theta_{\epsilon a} \frac{e^{ika}}{ika} \sum_{l=0}^{\infty} (2l+1) i^l j_l(kr') P_l(\cos \theta_{ar'}) \quad (5)$$

Here  $j_l(kr)$  is the incoming spherical Bessel function,  $P_l(\cos \theta)$  is the Legendre polynomial, and  $\vec{r}' = \vec{r} - \vec{a}$ . The scattering angle,  $\theta_{ar'}$ , is defined as the angle between the propagation vector for the incident plane wave,  $\hat{ka}$ , and the outgoing wave direction  $\vec{r}'$ .

To construct the scattered wave, we multiply each incoming partial wave by

$$T_l(k) = \frac{1}{2} (e^{2i\delta_l} - 1) = i \sin \delta_l e^{i\delta_l} \quad (6)$$

where  $\delta_\ell(k)$  is the partial wave phase shift. Summing the new outgoing wave gives

$$\psi_{\vec{a}}(\vec{r}') = \left(\frac{3}{4\pi}\right)^{1/2} \cos \theta_{\epsilon a} \frac{e^{ika}}{ika} \sum_{\ell=0}^{\ell_{\max}} (2\ell+1) T_\ell(k) i^\ell h_\ell(kr') P_\ell(\cos \theta_{a r'}) \quad (7)$$

The sum of  $\ell$  may be stopped at  $\ell_{\max}$  when all higher partial waves have negligible amplitude,  $|T_\ell(k)| \sim 0$ ,  $\ell > \ell_{\max}$ . At the angle resolved detector, located along  $\vec{R}$ , we may replace the outgoing spherical waves by their asymptotic limit. Then a scattering factor is defined by

$$f_{aR}(k) = \frac{1}{ik} \sum_{\ell=0}^{\ell_{\max}} (2\ell+1) T_\ell(k) P_\ell(\cos \theta_{aR}) \quad (8)$$

to give the scattered wave at the detector as

$$\psi_{\vec{a}}(\vec{R}) = \left(\frac{3}{4\pi}\right)^{1/2} \cos \theta_{\epsilon a} \frac{e^{ik|\vec{R}-\vec{a}|}}{ikR} \frac{e^{ika}}{a} f_{aR} \quad (9)$$

The factor  $\exp(ik|\vec{R}-\vec{a}|)$  corrects for the different origin of the scattered wave and for  $|\vec{R}| \gg |\vec{a}|$  we have  $|\vec{R}-\vec{a}| \sim |\vec{R}| - |\vec{a}| \cos \theta_{aR}$ .

The direct wave at the detector is

$$\psi_0(\vec{R}) = \left(\frac{3}{4\pi}\right)^{1/2} \cos \theta_{\epsilon R} \frac{e^{ikR}}{ikR} \quad (10)$$

and we calculate the ARPEFS oscillations due to a single atom as

$$\psi(k) = \frac{(\psi_0 + \psi_a)^* (\psi_0 + \psi_a)}{\psi_0^* \psi_0} = \frac{2|f_{aR}| \cos \theta_{\epsilon a}}{a \cos \theta_{\epsilon R}} \cos [ka(1 - \cos \theta_{aR}) + \phi_{aR}] \quad (11)$$

where  $f_{aR}(k) = |f_{aR}| \exp(i \phi_{aR})$ . This formula has been used to analyze experimental ARPEFS data in ref. 6.

## B. SPHERICAL WAVES

For spherical waves, the angular momentum expansion in its usual form is much more complex:<sup>11</sup>

$$ih_1(kr)Y_{10}(\hat{r}) = \sum_{\ell m n} G_{10\ell m n} i^{\ell n} j_{\ell n}(kr') Y_{\ell m n}(\hat{r}') \quad (12)$$

where  $\vec{r}' + \vec{a} = \vec{r}$ . This formula is the basis for Lee and Pendry's curved wave EXAFS formula.<sup>10</sup> To make physical arguments about the nature of curved wave corrections to the plane wave formula, we need a simpler form for this expansion, which we will refer to as an origin-shift addition theorem.

An alternative expansion for spherical waves may be derived most readily from Nozawa's original paper<sup>12</sup> which describes expansions of "Helmholtz's Solid Harmonics", his term for the product of spherical Bessel functions and spherical harmonics, which we will call "spherical waves". Nozawa demonstrated that the origin-shift addition theorem results when the raising operator for Helmholtz's Solid Harmonics,<sup>13</sup>

$$i^{\ell} h_{\ell}(kr) P_{\ell}^m(\cos \theta) e^{im\phi} = \left(\frac{-i}{k}\right)^m \left(\frac{\partial}{\partial x} + \frac{i\partial}{\partial y}\right)^m P_{\ell}^{(m)}\left(\frac{-i}{k} \frac{\partial}{\partial z}\right) h_0(kr) \quad (13)$$

is applied to the origin-shift addition theorem for  $h_0(kr)$ :

$$h_0(kr) = \sum_{\ell=0}^{\infty} (2\ell+1) i^{\ell} j_{\ell}(kr') i^{\ell} h_{\ell}(ka) P_{\ell}(\cos \theta_{ar'}) \quad (14)$$

Here  $P_{\ell}^{(m)}(-i\partial/k\partial z)$  is the operator obtained by using  $(-i\partial/k\partial z)$  as the argument of the  $m$ th derivative of the Legendre polynomial of order  $\ell$ . As we shall see, this differential form for the expansion eliminates the need for magnetic quantum numbers for the outgoing scattered wave and leaves explicit the angle dependence hidden within  $G_{\ell m \ell' m'}$  above.

For our particular case the raising operator formula is

$$ih_1(kr)P_1(\cos \theta) = \left(-\frac{i}{k} \frac{\partial}{\partial z}\right) h_0(kr) \quad (15)$$

and the origin-shift addition theorem becomes<sup>14</sup>

$$ih_1(kr)P_1(\cos \theta) = \sum_{\ell=0}^{\infty} (2\ell+1) i^{\ell} j_{\ell}(kr') h_0(ka)$$

$$* \{ d_1(ka) P_1(\cos \theta_{\epsilon a}) d_{\ell}(ka) P_{\ell}(\cos \theta_{ar'}) \}$$

$$-i \cos \theta_{\epsilon a} \frac{\partial d_{\ell}(ka)}{\partial(ka)} P_{\ell}(\cos \theta_{ar'})$$

$$-i \frac{(\cos \theta_{\epsilon r'} - \cos \theta_{\epsilon a} \cos \theta_{ar'})}{ka} d_{\ell}(ka) \frac{\partial P_{\ell}(\cos \theta_{ar'})}{\partial(\cos \theta_{ar'})} \quad (16)$$

We have introduced  $d_{\ell}(ka)$  to represent the polynomial part of the spherical Hankel function:

$$i^{l''} h_{l''}(ka) = \frac{e^{ika}}{ika} d_{l''}(ka) = h_0(ka) d_{l''}(ka) \quad (17)$$

Note that for large  $ka \gg l''(l''+1)$ ,  $d_{l''}(ka) = 1.0$ , and that  $d_l(ka)$  may be calculated by recursion:  $d_{l+1} = d_{l-1} - d_l(2l+1)/ika$ .

As before, the scattered wave may be calculated by multiplying each incoming partial wave amplitude by  $T_l(k)$  to generate an outgoing partial wave; each outgoing wave may be replaced by its asymptotic limit when the amplitude is calculated at the detector, position  $\vec{R}$ .

We invent a generalized scattering factor based on our origin-shift formula as

$$f_{aR}^{nm} = \frac{1}{ik} \sum_{l''=0}^{l''_{\max}} (2l''+1) T_{l''}(k) \frac{\partial^n d_{l''}(ka)}{\partial(ka)^n} \frac{\partial^m P_{l''}(\cos \theta_{aR})}{\partial(\cos \theta_{aR})^m} \quad (18)$$

and the scattered wave is then

$$\begin{aligned} \psi_a(\vec{R}) = & \left(\frac{3}{4\pi}\right)^{1/2} \frac{e^{ik|\vec{R}-\vec{a}|}}{ikR} \frac{e^{ika}}{a} \{d_1(ka) \cos \theta_{\epsilon a} f_{aR}^{00} \\ & - i \cos \theta_{\epsilon a} f_{aR}^{10} - \frac{i}{ka} f_{aR}^{01} [\cos \theta_{\epsilon R} - \cos \theta_{\epsilon a} \cos \theta_{aR}]\} \quad (19) \end{aligned}$$

If we label the factor within the braces  $F_{\text{SPH}} = |F| \exp(i\phi_{\text{SPH}})$  we parallel the plane wave construction of  $\chi(k)$  to find

$$\chi(k) = 2 \frac{|F_{\text{SPH}}|}{a \cos \theta_{\epsilon R}} \cos[ka(1 - \cos \theta_{aR}) + \phi_{\text{SPH}}] \quad (20)$$

Clearly,  $F_{\text{sph}}$  determines both the amplitude and phase of the oscillations we will measure. As  $ka$  becomes large, the factors  $f_{\text{aR}}^{10}$  and  $f_{\text{aR}}^{01}(ka)$  fall to zero,  $d_{\ell}(ka)$  becomes 1.0,  $f_{\text{aR}}^{00}$  tends to  $f_{\text{aR}}$ , and we have

$$F_{\text{SPH}} \rightarrow f_{\text{aR}} \cos \theta_{\text{ea}} \quad (21)$$

Thus by studying  $F_{\text{sph}}$  compared to  $f_{\text{aR}} \cos \theta_{\text{ea}}$  we can learn when curved wave corrections will influence the single scattering of photoelectrons.

An alternative derivation for this formula is outlined in Appendix A.

The same method may also be applied to calculation of oscillations in the total absorption cross section, the Extended X-ray Absorption Fine Structure (EXAFS). Here the scattered wave must be projected back onto the direct wave at the absorbing atom: the oscillations are an interference at the photoemitter. The derivation for (1s) core levels and polarized light is given in Appendix B. If we call

$$E_{\text{SPH}} = \frac{1}{ik} \sum_{\ell''=0}^{\ell_{\text{max}}} (2\ell''+1) T_{\ell''}(k) (-1)^{\ell''} \quad (22)$$

$$* \left\{ \cos^2 \theta_{\text{ea}} \left[ d_1(ka) d_{\ell''}(ka) - i \frac{\partial d_{\ell''}(ka)}{\partial(ka)} \right]^2 - \sin^2 \theta_{\text{ea}} \left[ \frac{d_{\ell''}(ka)}{ka} \right]^2 \frac{\ell(\ell+1)}{2} \right\}$$

then we compare  $E_{\text{sph}}$  to  $\cos^2 \theta_{\text{ea}} f_{\text{aR}}(\pi)$  to examine curved wave corrections for EXAFS.

We might proceed directly to numerical applications of these formulae, but the qualitative success of the plane wave approximation

suggests that some insight into electron scattering may be gained by examining the individual terms in these spherical wave formulas compared to results from a plane-wave model. We take up this topic in the next section.

### III. NATURE OF THE CURVED WAVE CORRECTIONS

In this section we examine the formulas derived in the previous section for the exact single scattering of  $l = 1$  spherical waves. We know that the plane wave scattering model is substantially correct so we concentrate on differences caused by allowing for wavefront curvature. We begin this section with a brief examination of the mathematical reduction of the spherical wave formulas to their plane wave limit. This provides one method for studying curved wave effects, but to be more specific we might inquire about the importance of the fundamental spherical nature of the waves which is independent of angular momentum - embodied in  $\exp(ikr)/ikr$  - compared to additional curved wave corrections due to the particular incident angular momentum. We will demonstrate that each term in the differential form, eqn 19, corresponds to specific curved wave corrections. The first term gives the basic correction common to all angular momenta, the second term corrects for additional radial structure specific to the incident angular momentum, while the third term corresponds to additional angular character specific to angular momentum.

Our curved wave formulas approach the plane wave results whenever the spherical Hankel functions can be replaced by their asymptotic limits (eqn. 3). In our notation this is equivalent to replacing the

polynomial part of the spherical Hankel function,  $d_l(ka)$  by 1.0 in our formulas:

$$d_l(ka) = \left[ 1 - \frac{l(l+1)}{2ika} + \dots \right] - 1.0 \quad (23)$$

Thus we must first discuss the size of  $l(l+1)/(2ika)$ . Notice that the angular momentum in this formula is the scattered wave angular momentum, not the dipole selection rule momentum from the photoabsorption.

The contribution of each partial wave to the final scattered wave is dictated by the partial wave amplitude (eqn. 6). For every wavenumber,  $k$ , there will be some angular momentum  $l_{\max}$  beyond which all partial wave amplitudes may be neglected. With some criterion for this cutoff we can define an equivalent range,  $r_0$ , for the scattering potential:<sup>15</sup>

$$l_{\max}(l_{\max} + 1) \sim (kr_0)^2. \quad (24)$$

In other words, the largest significant partial wave climbs in proportion to  $k$ . The asymptotic criterion then reads

$$\frac{kr_0}{2} \left( \frac{r_0}{a} \right) \ll 1 \quad (25)$$

for the last significant partial wave. By this analysis we conclude that the spherical Hankel function can be replaced by its limit only for large  $a \gg r_0$ ; higher energy actually leads us away from the limit. Of course, as the number of partial waves increases, the impact of the



largest angular momentum on the value of the scattering factor decreases. To properly assess this effect we should consider in detail the weight of each partial wave, but for a crude estimate assume equal weights. Then the contribution of the largest angular momentum decreases roughly like  $(1/l_{\max})$ , giving an asymptotic criterion for the sum as

$$\frac{1}{2} \left( \frac{r_0}{a} \right) \ll 1 \quad (26)$$

We expect  $r_0$  to be  $\approx 1A$  and for  $|\vec{a}|$  equal to the nearest neighbor distance,  $r_0/2a = 0.2$ . Under these assumptions the curved wave effects are not too small; we turn to study the curved wave formulas for ARPEFS and EXAFS.

For photoelectron scattering we have

$$F_{\text{SPH}} = d_1(ka) \cos \theta_{\epsilon a} f_{aR}^{00} - i \cos \theta_{\epsilon a} f_{aR}^{10} - i f_{aR}^{01} \left[ \frac{\cos \theta_{\epsilon R} - \cos \theta_{\epsilon a} \cos \theta_{aR}}{ka} \right] \quad (27)$$

The first term,

$$d_1(ka) \cos \theta_{\epsilon a} f_{aR}^{00} = \left[ 1 + \frac{i}{ka} \right] \frac{\cos \theta_{\epsilon a}}{ik} \sum_{\ell=0}^{\ell_{\max}} (2\ell+1) T_{\ell}(k) d_{\ell}(ka) P_{\ell}(\cos \theta_{aR}) \quad (28)$$

is the only one which survives in the asymptotic limit,  $ka \gg \ell(\ell+1)$ . By examining the origin-shift addition theorem for  $h_0(kr)$  (eqn 14) we can show that this first term corresponds to the single scattering of an  $\ell=0$  wave - the  $f_{aR}^{00}$  factor - multiplied by the  $\ell=1$  wave components--the  $d_\ell(ka) \cos \theta_{\epsilon a}$  part. The scattering factor,  $f_{aR}^{00}$ , differs from the plane wave counterpart,  $f_{aR}$ , only by including a weighting on partial waves,  $d_\ell(ka)$ , dependent on  $ka$ . Since  $h_0(ka) = \exp(ika)/ika$ , we can see that this weighting corrects the plane-wave scattering factor for the variation in the spherical wave over the finite size of the ion core potential due to  $(1/ika)$ .

The second term,

$$-i \cos \theta_{\epsilon a} f_{aR}^{10} = \frac{-i \cos \theta_{\epsilon a}}{ik} \sum_{\ell=0}^{\ell_{\max}} (2\ell+1) T_\ell(k) \frac{\partial d_\ell(ka)}{\partial(ka)} P_\ell(\cos \theta_{aR}) \quad (29)$$

contains the derivative of the polynomial part of the spherical Hankel function. The expansion of  $d_\ell$  in equation (23) gives the leading term in the derivative as

$$\frac{\partial d_\ell(ka)}{\partial(ka)} = \frac{1}{ika} \frac{\ell(\ell+1)}{2ika} \quad (30)$$

Since  $ka \sim 10$  in the ARPEFS energy range we can anticipate this spherical wave correction being much smaller than the difference between  $f_{aR}^{00}$  and  $f_{aR}$ : the factor  $\ell(\ell+1)/2ika$  represents the leading correction to the plane wave form and  $f_{aR}$  is smaller by  $1/ka$ . This term is literally the radial variation of  $f_{aR}^{00}$ : it corrects the S wave origin shift, given

by  $f_{aR}^{00}$ , for the variation in  $h_1(ka)$  over the potential not already contained in  $f_{aR}^{00}$ .

The third term,

$$\frac{-i}{ka} (\cos \theta_{\epsilon R} - \cos \theta_{\epsilon a} \cos \theta_{aR}) f_{aR}^{01} = \quad (31)$$

$$-i \frac{(\cos \theta_{\epsilon R} - \cos \theta_{\epsilon a} \cos \theta_{aR})}{(ka)(ik)} \sum_{\ell=0}^{\ell_{\max}} (2\ell+1) T_{\ell}(k) d_{\ell}(ka) \frac{\partial P_{\ell}(\cos \theta_{aR})}{\partial (\cos \theta_{aR})},$$

contains both an unusual angular factor and a derivative with respect to  $\cos \theta_{aR}$ . This term accounts for the variation in the spherical wave amplitude laterally across the width of the potential. We can use spherical trigonometry to rewrite this term in an instructive fashion. If we place three unit vectors in the directions of  $\hat{\epsilon}$ , the polarization vector,  $\vec{R}$ , the emission vector, and  $\vec{a}$ , the bond vector, at a common origin, then the vector tips will define a spherical triangle on a unit sphere with sides  $\theta_{\epsilon R}$ ,  $\theta_{\epsilon a}$ , and  $\theta_{aR}$ . Observing this triangle along the vector  $\vec{a}$  we see that

$$\cos \theta_{\epsilon R} - \cos \theta_{\epsilon a} \cos \theta_{aR} = \sin \theta_{\epsilon a} \sin \theta_{aR} \cos \phi_{\epsilon a R} \quad (32)$$

where  $\phi_{\epsilon a R}$  is the dihedral angle between  $\vec{\epsilon}$  and  $\vec{R}$  through  $\vec{a}$ . Since the associated Legendre polynomials are defined

$$P_{\ell}^m(\cos \theta) = \sin^m \theta \frac{d^m P_{\ell}(\cos \theta)}{d(\cos \theta)^m} \quad 0 \leq m \leq \ell \quad (33)$$

we can write

$$\begin{aligned}
 & -i \frac{(\cos \theta_{\epsilon R} - \cos \theta_{\epsilon a} \cos \theta_{aR})}{ka} f_{aR}^{01} & (34) \\
 & = \frac{\sin \theta_{\epsilon a} \cos \phi_{\epsilon a R}}{ik} \sum_{\ell=0}^{\ell_{\max}} (2\ell+1) T_{\ell}(k) d_{\ell}(ka) \frac{P_{\ell}^1(\cos \theta_{aR})}{ika}
 \end{aligned}$$

Thus this correction to the plane wave form reaches its maximum when the scattering potential is located in the nodal plane ( $\cos \theta_{\epsilon a} = 0$ ;  $\sin \theta_{\epsilon a} = 1$ ) of the outgoing spherical wave. The maximum size of  $P_{\ell}^1(\cos \theta_{aR})$  is  $(\ell+1)/2$  but all of the partial waves do not reach this maximum for the same angle. Nevertheless we can roughly say that this third term will peak near  $\theta_{aR} \sim 20^\circ$ , giving a curved wave correction approximately  $\ell(\ell+1)/2ka$  smaller than the first term.

To recap our assignment of the terms in the differential spherical wave formula to specific curved wave corrections, we associate the first term - containing  $f_{aR}^{00}$  - with the fundamental, angular-momentum-independent nature of the incident wave, the second term - containing  $f_{aR}^{10}$  - with radial corrections dependent on angular momentum, and the third term - containing  $f_{aR}^{01}$  - with angular corrections dependent on angular momentum. From this assignment, we can expect significant curved wave corrections to the single-scattering ARPEFS formula when

- i) the scattering potential is near a node in the incident wave angular distribution,
- ii) the scattering angle is near  $0^\circ$  (forward scattering), or
- iii) the scattering factor is near resonance.

We now consider these cases in more detail.

When the center of a scattering potential lies in a nodal surface of the incident wave, the plane wave model, eqn 11, predicts no scattering. For  $l=1$  incident waves, this geometry means  $\theta_{\epsilon a} = 90^\circ$  and  $\cos \theta_{\epsilon a} = 0$ . Thus only the third term of the differential formula is non-zero and thus this third term represents the entire curved wave correction for this geometry. It is interesting to note that the usual experimental geometries<sup>6</sup> for ARPEFS prevent this third term from producing its maximum effect. To maximize the measured photocurrent, the electron detector in the direction  $\vec{R}$ , is usually placed nearly parallel to  $\vec{\epsilon}$  ( $\theta_{\epsilon R} \sim 0^\circ$ ). If an atom has  $\theta_{\epsilon a} = 90^\circ$  so that  $\sin \theta_{\epsilon a} = 1$ , then the scattering angle,  $\theta_{aR}$ , must also be  $\sim 90^\circ$  for the scattered wave to enter the detector: for this experimental geometry the condition ( $\theta_{\epsilon a} = 90^\circ$ ,  $\theta_{aR} \sim 20^\circ$ ) will never be satisfied.

Just the opposite must be true for the unusual experimental geometry adopted by Sinkovic et al., in a recent Azimuthal Photoelectron Diffraction experiment<sup>16</sup>. They selected  $\theta_{\epsilon R} = 72^\circ$  and measured electrons emitted  $10^\circ$  from the surface: many of the important forward scattering atoms would have  $\sin \theta_{\epsilon a} > .5$ ,  $\cos \phi_{\epsilon a R} = 1$ , and  $\theta_{aR} \sim 20^\circ$ . Thus their observation that plane-wave calculations gave poor agreement with experiment may reflect the neglected variation in wave amplitude across the scattering potential rather than multiple scattering effects.

When the scattering angle is near  $0^\circ$  we can get large curved-wave corrections strictly from the difference between the first term containing  $f_{aR}^{00}$  and the plane wave limit. To demonstrate this we expand  $d_l(ka)$  according to equation 23, and subtract the asymptotic plane-wave part:

$$(f_{aR}^{OO} - f_{aR}^{PLANE}) \sim \frac{1}{ik} \sum_{\ell=0}^{\ell_{\max}} (2\ell+1) T_{\ell}(k) \left[ \frac{\ell(\ell+1)}{2ika} \right] P_{\ell}(\cos \theta_{aR}) \quad (35)$$

The maximum difference will occur for forward scattering since  $P_{\ell}(1) = 1$  and all the partial wave corrections add. Conversely the minimum curved wave corrections should be expected for backscattering since  $P_{\ell}(-1) = (-1)^{\ell}$  and successive partial waves tend to cancel. This overall description should be most accurate for higher energies where the partial wave amplitudes,  $T_{\ell}(k)$ , have little structure.

When the full scattering factor approaches zero near a Generalized Ramsauer Townsend resonance<sup>17</sup> we can expect the third case for large curved wave corrections. For special values of electron wavevector,  $k$ , and scattering angle,  $\theta_{aR}$ , the partial wave sum will be zero due to exact cancellation of all partial wave components. The particular pair of values  $(k, \theta_{aR})$  at which the scattering factor becomes zero will differ between the plane-wave and spherical-wave models as they weight the individual partial waves differently. Thus analysis of scattering resonance data with a plane-wave model will give incorrect scattering angles and the observed resonance energy position will not be correctly given by plane wave calculations. While the first two circumstances leading curved wave effects discussed above involve only one or another of the terms in the formula, the resonance calculation will depend in detail on all three terms.

Curved wave corrections to the EXAFS formula are directly analogous to the corrections for photoelectron diffraction. Since the "detector" for EXAFS is the photoemitting atom, the curved wave effects are

squared: our detector is not asymptotically far from the scattering atom. The first term of the spherical wave scattering factor

$$\frac{\cos^2 \theta_{\epsilon a}}{ik} \sum_{\ell=0}^{\ell_{\max}} (2\ell+1) T_{\ell}(k) (-1)^{\ell} \left[ d_{\ell}(ka) d_{\ell}'(ka) - i \frac{\partial d_{\ell}(ka)}{\partial(ka)} \right]^2 \quad (36)$$

has the same angular dependence as the plane wave model. This term contains both the basic radial correction for  $1/ika$ --the first factor inside the brackets--and the radial derivative correction. As discussed above, the radial derivative factor is usually much smaller than the s-wave origin-shift.

The second term of the EXAFS spherical wave amplitude factor has the opposite angular dependence compared to a plane wave model:

$$\frac{\sin^2 \theta_{\epsilon a}}{ik} \sum_{\ell=0}^{\ell_{\max}} (2\ell+1) T_{\ell}(k) (-1)^{\ell} \left[ \frac{d_{\ell}(ka)}{ka} \right]^2 \frac{\ell(\ell+1)}{2} \quad (37)$$

This term corrects for variation in the incident wave amplitude across the potential, primarily due to the node in the p wave angular distribution. Thus for atoms along the nodal plane perpendicular to the electric vector, this term represents the error made by neglecting the angular structure in the photoelectron wave.

Typically EXAFS analysis is not concerned with relative scattering amplitude of individual atoms. Most of the measurable signal comes from nearest neighbor atoms, all of which contribute oscillations of the same frequency. The overall EXAFS amplitude is not simply given by the magnitude of the scattering amplitude<sup>18,19</sup> and hence the spherical wave

corrections to the magnitude are of little consequence. Rather it is the phase of the scattering factor that is central to the EXAFS analysis and high precision should require spherical wave correction; the weight of the individual partial waves in the scattering factor sum will otherwise be incorrect. Of course, practical EXAFS analysis does not rely on the accuracy of the theoretical scattering factor: empirical phase shifts are nearly always derived from known model compounds.

An important EXAFS technique which does rely on relative scattering amplitudes is the polarization dependence employed to determine structures on surfaces.<sup>20</sup> Here the overall amplitude for nearest neighbors is measured for several orientations of the polarization vector with respect to the crystalline sample axis. The results are usually fitted to the angular distribution predicted by a plane wave model-- $\cos^2 \theta_{ea}$ --and ignores spherical wave effects. We would expect the largest curved wave correction when  $ka$  is small, i.e. low Z elements having short bond lengths and in the lower energy region, and when we need accurate angular distribution calculations for small  $\cos^2 \theta_{ea}$ .

Looking back at the EXAFS formula we also find some insight into the success of the plane wave model. The leading correction to the plane wave amplitude is

$$\Delta = \left[ \frac{E_{SPH}}{\cos^2 \theta_{ea}} - f_{aR}^{plane}(\pi) \right] - \frac{1}{ik} \sum_{l=0}^{l_{max}} (2l+1) T_l(k) (-1)^l \frac{l(l+1)}{ika} \quad (38)$$

This term is just twice the correction for backscattering ARPEFS, and, as we argued above, the successive terms tend to cancel. Furthermore, we can make a crude argument that the  $k$  dependence--and hence the



frequency shift--of this correction will be very small. The factor  $l(l+1)/ika$  strongly favors high angular momentum waves. If we define an impact parameter  $b = l/k$ , we can take a semiclassical approximation for the phase shift:<sup>21</sup>

$$\delta_l(k) = \frac{Z(b)}{kr_0} \quad (39)$$

Here,  $Z(b)$  is the unscreened nuclear charge within a sphere of radius  $b$  around the scattering atom. For large  $l$  we assume small phase shifts to write

$$T_l(k) = i\delta_l(k) = \frac{iZ_l(b)}{kr_0} \quad (40)$$

and since  $l \gg 1$  we have

$$\Delta = \sum_{l=0}^{l_{\max}} \frac{2l}{ik} \frac{Z_l(b)}{kr_0} (-1)^l \frac{l^2}{ka} \quad (41)$$

To get a series whose limit does not depend on  $k$  we invent a sampling radius

$$r_n = \frac{l_{\max-n}}{k} \quad (42)$$

which coincides with  $l_{\max} = kr_0$  for  $l_{\max} \gg 1$ . Then

$$\Delta \approx \sum_{n=0}^{l_{\max}} \frac{2r_n^3}{ir_0^a} Z(r_n) (-1)^{l_{\max}-n}$$

Since the  $r_n$  are constants of the potential, this spherical wave correction is roughly independent of  $k$ . Note that this argument requires the low angular momentum to be insignificant and we may not conclude that  $f_{aR}^{00}$  or  $f_{aR}$  are roughly independent of  $k$  by similar steps.

#### IV. CURVED WAVE CORRECTIONS TO THE SCATTERING FROM Ni ATOMS

Now we turn to some specific examples of curved wave effects in the scattering of electrons from Ni atoms. We will begin by examining the angle dependence of the scattering factors at  $5\text{\AA}^{-1}$  (95 eV) and at  $10\text{\AA}^{-1}$  (381 eV), followed by their  $k$  and  $r$  dependences. For each case we will compare  $f_{aR}^{00}$  to the plane-wave limit,  $f_{aR}$ . As the last example we calculate the effect of curved wave corrections to the polarization dependence in surface EXAFS. In all these examples we take  $|\vec{a}| = 2.23\text{\AA}$ .

Figure 1 compares the amplitudes of  $f_{aR}^{00}$  and  $f_{aR}$  for scattering angles from  $0$ - $180^\circ$  at a wavenumber of  $5\text{\AA}^{-1}$  (see eqn. 28). The general trend confirms our qualitative discussion in the previous section: the largest corrections are in the forward scattering directions. Figure 2 gives the amplitude of  $f_{aR}^{10}$  (eqn. 29); note the dramatic reduction in magnitude. The angular structure of  $f_{aR}^{10}$  is rather similar to  $f_{aR}^{00}$ .

The angular spherical wave correction, eqn. 31, is plotted in figure 3 as  $|\sin \theta_{aR} f_{aR}^{01}|$  to emphasize the fact that this correction is zero for forward ( $\theta_{aR} = 0^\circ$ ) and exactly backscattering ( $\theta_{aR} = 180^\circ$ ). The overall scale is 20 percent of the scale in figure 7, but recall

that two additional angle factors,  $\sin \theta_{\epsilon a}$  and  $\cos \phi_{\epsilon a R}$  reduce this correction unless the scattering geometry is special.

We have constructed figures 4, 5, and 6 to parallel figures 1, 2, and 3, respectively, except  $k = 10\text{\AA}^{-1}$  for these new figures. All three comparisons demonstrate that the curved wave corrections are not much smaller at this higher energy, but the cancellation of successive angular momenta due to  $P_l(\cos\theta) \approx (-1)^l$  is much more effective. Thus all the large scattering-angle ( $\theta > 90^\circ$ ) amplitudes are quite accurate (5 percent) in the plane wave model, while the amplitude for scattering through  $32^\circ$  is too high by more than a factor of 2.

We can also compare the scattering factor phase by plotting the argument of the complex ratio  $f_{aR}^{00}/f_{aR}$ , i.e. their phase difference, as in Figure 7. For  $k = 5\text{\AA}^{-1}$ , the phase difference is roughly  $+0.5$  radians; note that the two angles where the phase difference is not near  $+0.5$  radians correspond to scattering angles with small scattering amplitudes, see figure 1. The curve for  $k = 10\text{\AA}^{-1}$  has the same behavior although the shift is about half as large.

The  $k$  dependence of these scattering factors is illustrated for  $\theta_{aR} = 173^\circ$  in figure 8,  $\theta_{aR} = 0^\circ$  in figure 9, and  $\theta_{aR} = 127^\circ$  in figure 10. The backscattering geometry, figure 8, is the most important one for ARPEFS and, fortunately, the plane wave model is rather accurate. As we noted above, the angular curved wave correction is eliminated by  $\sin \theta_{aR} \approx 0$  for backscattering, and figure 8 shows that  $f_{aR}^{10}$  is very much smaller than  $f_{aR}^{00}$ . Thus  $f_{aR}^{00}$  by itself characterizes the backscattering of  $l=1$  waves. Notice also that the plane wave amplitude error approaches a constant not equal to zero, for large  $k$ . This is explained in the same manner as the EXAFS discussion in the previous section.

The greatest curved wave corrections occur in the forward directions; figure 9 gives the example of  $\theta_{aR} = 0^\circ$ . The plane wave amplitude is roughly  $.2A$  too small over the entire range in  $k$ . Without the alternating sign of  $P_\ell(-1)$  characteristic of backscattering, we see no approach to the plane wave limit at large  $k$ . Again  $f_{aR}^{10}$  is very small, at least a factor of 20 below  $f_{aR}^{00}$ ;  $f_{aR}^{01}$  cannot contribute to forward scattering as long as  $\theta_{aR} < \sim 10^\circ$ . The phase difference (not plotted) between  $f^{00}$  and  $f_{aR}^{\text{plane}}$  is  $\sim .7$  radians.

Finally, we consider scattering through  $127^\circ$ , the position of a Generalized Ramsauer Townsend resonance in Ni. The resonance is a crossing of the origin in the complex plane by the complete scattering factor. The resonance position in energy and angle depends crucially on the cancellation of many partial waves and hence cannot be correctly predicted with a plane wave calculation. Figure 10 displays the scattering factors for  $\theta_{aR} = 127^\circ$ . The factors  $|f_{aR}^{00}|$  and  $|f_{aR}^{\text{plane}}|$  are reasonably close except in the resonance region near  $8A^{-1}$ . The angular curved wave correction is now significant, especially since it conspires with  $f_{aR}^{00}$  to make the overall scattering amplitude zero at  $k = 7.5A^{-1}$ . ( $f_{aR}^{10}$  has not been plotted; it is very small for  $\theta_{aR} = 127^\circ$ ). The difference between exact single-scattering and plane-wave calculations is more dramatic in the phase of the scattering factor. Calculations done for values of  $ka$  corresponding to recent experimental measurements<sup>17</sup> are shown in figure 11. The phase jump at resonance is not correctly placed in angle or energy in the plane wave limit.

To estimate the distance,  $|\vec{a}|$ , beyond which we can safely use the plane wave formula, we plot in figure 12 the radius at which  $|f_{aR}^{00} - f_{aR}^{\text{plane}}| \leq 0.06A$ , for two energies,  $k = 5A^{-1}$  and  $k = 10A^{-1}$ . This

criterion for the allowable error in scattering factor was chosen to be ~ 10 percent of the backscattering ( $\theta_{aR} = 180^\circ$ ) amplitude for Ni. We see from this figure that plane wave calculations are never adequate by this criterion for forward scattering at any energy or any practical radius. For angles greater than  $45^\circ$ , most scattering atoms within 10Å of the photoemitter would require curved wave corrections in the lower energy region, while perhaps only the nearest neighbors require these extra calculations for  $k = 10\text{Å}^{-1}$ .

To discuss an example calculation for the curved wave EXAFS formula, we adopt the second form for  $\chi(k)$  given in Appendix B, eqn. (B13). Figure 13 compares  $f^{iso}$  to its asymptotic limit  $f^{plane}(\pi)$  and to  $f^{an}$ . We see a close analogy between  $f^{iso}$  for EXAFS and  $f_{aR}^{00}$  for ARPEFS, but the curved wave corrections are larger for EXAFS (compare figure 8) since the "detector" is not asymptotically far from the scattering atom. Once again the large  $k$  region approaches a non-zero constant plane-wave error. Perhaps most interesting,  $|f^{an}|$  is seen to be nearly two orders of magnitude smaller than  $|f^{iso}|$  in this energy range. Thus, at least for Ni atoms, the standard EXAFS formula with  $f^{iso}$  replacing  $f^{plane}(\pi)$  would give 1 percent accurate curved wave results. Furthermore, since the polarization dependence technique relies only on the assumption that the oscillations are proportional to  $\cos^2 \theta_{ea}$ , curved wave corrections to the calculated amplitude ratios are entirely insignificant.

## V. DISCUSSION

We have derived new formulae and given examples for the curved wave scattering of  $l=1$  spherical waves. What can we expect for more general spherical waves? We offer some qualitative ideas in this section.

We envision two important cases: i) photoabsorption by p, d, and f core levels giving spherical waves with higher angular momenta and magnetic sublevel occupations; and ii) multiple scattering preceded either by photoelectron scattering or plane wave scattering typical for the LEED experiment. Both of these problems can be approached by the method we use here for  $l=1$  waves. That is, the origin-shift addition theorem summed over magnetic sublevels can be differentiated to higher and higher order. The resulting expressions will be formidable so we will be content with estimates for now.

First we consider higher  $l$  waves populated by photoemission. For core orbital initial states with p, d, or f orbital angular momentum, two partial waves with  $l \pm 1$  will be created. Each partial wave may be treated by the method of section II. We should always get a first term like  $d_l(ka)Y_{lm}(a)f_{aR}^{00}$ , the amplitude of the  $l$  spherical wave times the scattering factor for  $l=0$  waves. This is the only curved wave factor which survives the asymptotic limit and hence will always be the most important. Our discussion for  $l=1$  virtually ignores  $d_l(ka)$  as being close to 1.0, but for higher angular momenta this factor may be important. Otherwise, this first term will follow the trends discussed in the previous section.

We should also always get curved wave corrections due to differences between the  $(1/ikr)$  dependence of  $h_0(kr)$  and the angular-momentum-dependent radial wave character through the potential region - corrections analogous to  $f_{aR}^{10}$ . For higher angular momenta, the difference between the radial character of the incident spherical wave and the radial character of  $h_0(ka)$  already included in the first term will increase. We might conclude from our Ni example calculations that

these radial variations are negligible for  $\ell=1$  waves; for some higher  $\ell$  we will be forced to include this term.

For all  $\ell$ , the radial variations should be less than the angular variations simply because spherical waves (except  $\ell=0$ ) have stronger angle dependence. Thus curved wave corrections analogous to  $f_{aR}^{01}$  will be increasingly important for higher angular momenta. These angular corrections are always greatest near nodes in the incoming wave, where the wave amplitude is changing most rapidly. The nodal regions has the least amplitude and the finite extent of the potential is anyway averaging opposite phase waves across the nodal surface, smoothing out the nodal structure. Hence, on the average, even these angular corrections will not be large. The phrase "on the average" is connected with the additional angular vectors like  $\sin \theta_{\epsilon a} \sin \theta_{aR} \cos \phi_{\epsilon aR}$  which multiply the curved wave angular correction.

In addition to more significant curved wave corrections of the same type as the  $\ell=1$  wave, higher angular momenta waves should also have corrections corresponding to higher order derivatives. Thus the second derivatives of the incoming wave across the extent of the potential will become important for some high  $\ell$ . Actual calculations are necessary to determine how important these corrections will be.

This leads us to the second important case, multiple scattering. While photoabsorption can populate only dipole allowed angular momenta, an outgoing scattered wave contains all angular momenta up to  $\ell_{\max} - kr_0$ . To apply the method of this paper to the exact multiple scattering of spherical waves would--as a practical matter--require automation of the derivative calculations, a dubious improvement over the Gaunt integral summation formula, equation 12. On the other hand, the

outgoing scattered wave is no more than a spherical wave with an angular dependence and phase determined by scattering rather than by photoabsorption. Thus, approximate multiple scattering could be calculated by starting with  $f_{aR}^{00}$  times the single scattered wave amplitude at the second scattering center and adding curved wave corrections by numerical differentiation of the single-scattered wavefunction.

## VI. CONCLUSION

To summarize our work, we have

- i) derived new curved wave formulae for single scattering of (1s) core level photoelectrons, appropriate for ARPEFS and EXAFS experiments,
- ii) interpreted the individual scattering factors in this formula as different types of curved-wave corrections, allowing some guidelines to be devised to predict which scattering problems require curved-wave formulas,
- iii) given some idea of the size of these factors for Ni atom scattering, and
- iv) discussed the possible generalization to higher angular momenta core levels.

The significance of these results is partly formal and partly practical. The remarkable accuracy of the plane wave model has been widely recognized,<sup>4,22</sup> but often attributed to the asymptotic limit of the spherical wave. Our new formulas more clearly demonstrate the origin of this convenience: the improved cancellation of partial waves



at large  $k$ . Thus the accuracy of the plane wave model does not improve for large  $k$  in forward scattering directions. This point may also be made by a semi-classical argument. As figure 14 illustrates, forward scattering corresponds to large classical impact parameters;<sup>21</sup> backscattering corresponds to low enough impact parameter to sample the strong attractive center region of the potential. The wavefront curvature corrections are thus much larger for forward scattering directions which sample the extreme edges of the potential.

On the practical side, our new curved-wave formulas are scarcely more complicated than the plane-wave versions. Some advantage may also be made of the different angle dependences of each scattering factor, to minimize numerical computations. Hopefully, our qualitative discussion and numerical example will serve as some guide to estimate when curved wave effects may be important. Finally, we have demonstrated that curved wave EXAFS calculations can be quite accurate with only a minor modification of the plane-wave formula, a result which extends the recent work of Schaich<sup>23</sup> and of Gurman, et al.<sup>24</sup>

Unfortunately, it is also clear from our results that curved wave effects cannot explain the difference between ARPEFS experiments and the single-scattering plane-wave calculations of Bullock, Fadley, and Orders.<sup>7</sup> The curved wave corrections are typically - 20 percent and only that large in the forward directions. Thus while we have reduced the computational barrier to using curved wave calculation for ARPEFS, we can also conclude that the major discrepancies between theory and experiment are not due to curved wave corrections at least for single backscattering.

We can characterize the disagreement between model calculations and ARPEFS measurement by noting that scatterings from nearest neighbors and backscatterings from non- nearest neighbors appear to be much more dominant than predicted theoretically. Wavefront curvature increases scattering for some angles, decreases it for others and generally has less effect for backscattering. Therefore, while curved wave formulas may be important for accurate calculation, there are larger errors elsewhere in the theory. Multiple scattering must be part of the answer: as figure 4 illustrates, forward scattering is large in the ARPEFS energy range and should not be neglected. Our results here predict that this forward scattering cannot be calculated within the plane wave formulation. There may also be errors in the inelastic scattering and thermal averaging. We must investigate these questions in further work.

APPENDIX A: ALTERNATE DERIVATION FOR DIFFERENTIAL FORM OF ORIGIN-SHIFT  
ADDITION THEOREM

We may arrive at the results of section II by an entirely different route. We will use a series of well known formulas conveniently tabulated in Pendry,<sup>1</sup> his appendix A.

We begin with the origin-shift addition theorem for  $(l,m) = (1,0)$ , equation 12. Using the definition of  $Y_{10}$  and the recursion relation for  $Y_{lm}$  we find

$$G_{10, l''m''} = 4\pi \sum_{l', m'} i^{l'} h_{l', (ka)} Y_{l', m'}^*(\hat{a}) \left\{ \left( \frac{3}{4\pi} \right)^{1/2} A_{l''+1, -m''}^0 \right. \quad (A1)$$

$$\left. \int Y_{l', m'}(\hat{K}) Y_{l''+1, m''}^*(\hat{K}) d\Omega_K + \left( \frac{3}{4\pi} \right)^{1/2} A_{l'', -m''}^0 \int Y_{l', m'}(\hat{K}) Y_{l''-1, m''}^*(\hat{K}) d\Omega_K \right\}$$

In other words, since  $Y_{10}$  is proportional to  $\cos(\theta)$ , the product  $Y_{10} Y_{l''}^*$  becomes the recursion relation for  $Y_{l''m''}$ . The factor

$$A_{lm}^0 = \left[ \frac{(l+m)(l-m)}{(2l+1)(2l-1)} \right]^{1/2} \quad (A2)$$

is related to the ratios of the normalizing coefficients of spherical harmonics. The remaining integrals in  $G_{10, l''m''}$  are the orthonormality conditions for spherical harmonics;

$$\int Y_{l', m'}(\hat{K}) Y_{l''+1, m''}(\hat{K}) d\Omega_K = \delta_{l', l''+1} \delta_{m', m''} \quad (A3)$$

and the sum on  $l', m'$  simplifies to

$$G_{10, \ell'' m''} = \left(\frac{3}{4\pi}\right)^{1/2} 4\pi \{ A_{\ell'+1, -m''}^0 i^{\ell''+1} h_{\ell''+1}(ka) Y_{\ell''+1, m''}^*(\hat{a}) + A_{\ell'', -m''}^0 i^{\ell''-1} h_{\ell''-1}(ka) Y_{\ell''-1, m''}^*(\hat{a}) \} \quad (A4)$$

The factor inside the braces is the result of a differential operation on  $i^{\ell''} h_{\ell''}(ka) Y_{\ell'', m''}^*$ . Rewriting Nozawa's<sup>12</sup> equation 3.8 in terms of normalized spherical harmonics shows that

$$\left(-i \frac{\partial}{k \partial z}\right) i^{\ell''} h_{\ell''}(ka) Y_{\ell'' m''}^*(\hat{a}) = \{ A_{\ell''+1, -m''}^0 i^{\ell''+1} h_{\ell''+1}(ka) Y_{\ell''+1, m''}^*(\hat{a}) + A_{\ell'', -m''}^0 i^{\ell''-1} h_{\ell''-1}(ka) Y_{\ell''-1, m''}^*(\hat{a}) \} \quad (A5)$$

Thus

$$G_{10 \ell'' m''} = \left(\frac{3}{4\pi}\right)^{1/2} 4\pi \left(-i \frac{\partial}{k \partial z}\right) i^{\ell''} h_{\ell''}(ka) Y_{\ell'' m''}^*(\hat{a}) \quad (A6)$$

with

$$\begin{aligned} \left(\frac{\partial}{k \partial z}\right) &= \cos \theta_{\epsilon a} \frac{\partial}{k(\partial a)} - \frac{\sin \theta_{\epsilon a}}{ka} \frac{\partial}{\partial \theta_{\epsilon a}} \\ &= \cos \theta_{\epsilon a} \frac{\partial}{k(\partial a)} - \frac{(\cos \theta_{\epsilon R} - \cos \theta_{\epsilon a} \cos \theta_{aR})}{(ka)} \frac{\partial}{\partial(\cos \theta_{aR})} \end{aligned} \quad (A7)$$

The addition theorem for spherical harmonics then leads to the results in equation (19). We can avoid the derivative operation altogether by

applying the recursion formulas for  $h_{\ell}''$  and  $Y_{\ell}''m''$ , but this approach is tedious.

## APPENDIX B. APPLICATION TO EXAFS

We apply the approach of section II to the spherical-wave single-scattering Extended X-ray Absorption Fine Structure. Schaich<sup>23</sup> and Gurman, et al.<sup>24</sup> recently derived simplified, exact EXAFS formulas for cubic or polycrystalline environments. Here we consider only (1s) core-level excitation and linearly polarized light, but we allow a general environment. With the  $\hat{z}$  axis along the polarization vector, the dipole selection rules reduce Schaich's equation (3) for the x-ray absorption coefficient to

$$\mu_c = A_4 \text{Im}[M_{01}^2 (i + \chi_1)] \quad (\text{B1})$$

Our  $\chi_1$  corresponds to Schaich's  $(i + \chi_{11})$ . We are interested only in the oscillations,  $\chi_1$ ; we refer to Schaich for the radial matrix elements  $M_{01}$  and constants in  $A_4$ . Transcribing Schaich's equation (5) into our notation gives

$$\chi_1(k) = \sum_{\vec{a} \neq 0} \sum_{\ell "m"} [e^{i\delta'_1} (i) G_{\ell "m" 10}(-k\vec{a}) (-i) T_{\ell "m"}(k) G_{10\ell "m"}(k\vec{a}) (-i) e^{i\delta'_1}] \quad (\text{B2})$$

The factor  $e^{i\delta'_1}$  is the absorber atom phase shift which cancels in the photoelectron diffraction experiment and hence was dropped from the formulas of section II.

To apply the differential form from appendix A, note that

$$G_{\ell''m''10}(-\vec{ka}) = (-1)^{m''} G_{10\ell''-m''}(-\vec{ka}) \quad (B3)$$

This is a consequence of the conjugation property of spherical harmonics

With the differential forms for the origin-shift addition theorem coefficients, we have

$$\begin{aligned} \chi_1(k) = & \sum_{\vec{a}(\neq\vec{0})} 3e^{i2\delta_1'} \sum_{\ell''} \left(\frac{1}{ik} \frac{\partial}{\partial z'}\right) \left(\frac{1}{ik} \frac{\partial}{\partial z}\right) \sum_{m''} 4\pi i^{\ell''} h_{\ell''}(ka') Y_{\ell''m''}(\hat{a}') \\ & (-i) T_{\ell''}(k) i^{\ell''} h_{\ell''}(ka) Y_{\ell''m''}^*(\hat{a}) \end{aligned} \quad (B4)$$

The primes distinguish outgoing and backscattered waves until the derivatives are complete. The addition theorem for spherical harmonics simplifies this expression, and we employ our separation of spherical waves into asymptotic and polynomial parts to write

$$\begin{aligned} \chi_1(k) = & - \sum_{\vec{a}(\neq\vec{0})} 3e^{i2\delta_1'} \sum_{\ell''} (2\ell''+1) \left(\frac{1}{ik} \frac{\partial}{\partial z'}\right) h_0(ka') d_{\ell''}(ka') \\ & \left(\frac{1}{ik} \frac{\partial}{\partial z}\right) h_0(ka) d_{\ell''}(ka) P_{\ell''}(\cos \theta_{aa'}) \end{aligned} \quad (B5)$$

where  $\cos \theta_{aa'}$  will ultimately be  $-1$ . The first derivative becomes

$$\begin{aligned} & \left(\frac{1}{ik} \frac{\partial}{\partial z}\right) h_0(ka) d_{\ell''}(ka) P_{\ell''}(\cos \theta_{aa'}) \\ & = h_0(ka) \{d_1(ka) d_{\ell''}(ka) \cos \theta_{aa'} P_{\ell''}(\cos \theta_{aa'})\} \end{aligned}$$

$$\begin{aligned}
& + \frac{\cos \theta_{\epsilon a}}{ik} \frac{\partial d_{\ell}''(ka)}{\partial(a)} P_{\ell}''(\cos \theta_{\epsilon a'}) \\
& + \frac{(\cos \theta_{\epsilon a'} - \cos \theta_{\epsilon a} \cos \theta_{\epsilon a'})}{ika} d_{\ell}''(ka) \frac{\partial P_{\ell}(\cos \theta_{aa'})}{\partial(\cos \theta_{aa'})} \} \quad (B6)
\end{aligned}$$

The first term in this expression is a consequence of the derivative as a lifting operator. After the second derivative we may set  $a' = a$ ,  $P_{\ell}(\cos \theta_{aa'}) = (-1)^{\ell}$ , and  $[\cos \theta_{\epsilon a'} - \cos \theta_{\epsilon a} \cos \theta_{aa'}] = 0$ . We also need the value of  $dP_{\ell}(x)/dx$  for  $x = (-1)$ ; it is equal to  $(-1)^{\ell+1} \ell(\ell+1)/2$ . Thus we have

$$x_1(k) = - \sum_{\vec{a}(\neq \vec{0})} 3e^{i2\delta_1} \frac{e^{i2ka}}{ka^2} \frac{1}{ik} \sum_{\ell=0}^{\ell_{\max}} (2\ell+1) T_{\ell}(k) (-1)^{\ell} \quad (B7)$$

$$\left\{ \cos^2 \theta_{\epsilon a} [d_1(ka) d_{\ell}(ka) - i \frac{\partial d_{\ell}(ka)}{\partial(ka)}]^2 - \frac{\sin^2 \theta_{\epsilon a}}{(ka)^2} [d_{\ell}(ka)]^2 \frac{\ell(\ell+1)}{2} \right\}$$

This form most clearly displays the origin of the curved wave corrections, but to compare to the work of Schaich, note that

$$\frac{1}{ik} \frac{\partial d_{\ell}(ka)}{\partial(a)} = d_{\ell-1}(ka) - d_{\ell}(ka) - \frac{\ell}{ika} d_{\ell}(ka) \quad (B8)$$

which--together with the recursion relation for  $d_{\ell}(ka)$ --shows that

$$[d_1(ka) d_{\ell}(ka) + \frac{1}{ik} \frac{\partial d_{\ell}(ka)}{\partial(a)}] = \left[ \frac{\ell+1}{2\ell+1} d_{\ell+1} + \frac{\ell}{2\ell+1} d_{\ell-1} \right] \quad (B9)$$



The square of this factor may be reduced with the help of the square of the recursion relation for  $d_\ell$  to give

$$\left[ \frac{\ell+1}{2\ell+1} d_{\ell+1} + \frac{\ell}{2\ell+1} d_{\ell-1} \right]^2 = \left[ \frac{\ell+1}{2\ell+1} d_{\ell+1}^2 + \frac{\ell}{2\ell+1} d_{\ell-1}^2 + \frac{\ell(\ell+1)}{(ka)^2} d_\ell^2 \right] \quad (\text{B10})$$

Then we can define

$$f^{\text{ISO}}(\pi) = \frac{1}{ik_1} \sum_{\ell=0}^{\ell_{\text{max}}} (2\ell+1) T_\ell(k) (-1)^\ell \left[ \frac{\ell+1}{2\ell+1} d_{\ell+1}^2 + \frac{\ell}{2\ell+1} d_{\ell-1}^2 \right] \quad (\text{B11})$$

and

$$f^{\text{an}}(\pi) = \frac{1}{ik_1} \sum_{\ell=0}^{\ell_{\text{max}}} (2\ell+1) T_\ell(k) (-1)^\ell \frac{\ell(\ell+1)}{(ka)^2} d_\ell^2(ka) \quad (\text{B12})$$

to write

$$\chi(k) = \text{Im} \left\{ - \sum_{a(\neq 0)} 3 \frac{e^{12ka}}{ka^2} e^{i2\delta_1'} \left[ (f^{\text{ISO}} + f^{\text{an}}) \cos^2 \theta_{\epsilon a} - \frac{f^{\text{an}}}{2} \sin^2 \theta_{\epsilon a} \right] \right\} \quad (\text{B13})$$

In an isotropic or cubic environment,  $2 \cos^2 \theta_{\epsilon a} = \sin^2 \theta_{\epsilon a}$  and the anisotropic scattering factor cancels out to give the same formula derived by Schaich<sup>23</sup> and by Gurman et al<sup>24</sup>. Notice that our result demonstrates that the simplification achieved by these authors is not a consequence of symmetry--the general formula is scarcely more complicated than the high symmetry version--but rather is a result of summing over the equivalent magnetic sublevels of the scattered wave.

## ACKNOWLEDGEMENTS

This work was supported by the Director, Office of Energy Research, Office of Basic Energy Sciences, Chemical Sciences Division of the U.S. Department of Energy under Contract No. DE-AC03-76SF00098.

## REFERENCES

1. J.B. Pendry, Low Energy Electron Diffraction. Academic Press, London, (1974).
2. M.A. Van Hove and S.Y. Tong, Surface Crystallography by LEED, Springer-Verlag (1979).
3. C.B. Duke, Adv. Chem. Phys., 27, 1, (1974).
4. P.A. Lee, P.H. Citrin, P. Eisenberger, and B.M. Kincaid, Rev. Mod. Phys. 53, 769 (1981).
5. P.A. Lee, Phys. Rev. B 13, 5261 (1976).
6. J.J. Barton, C.C. Bahr, Z. Hussain, S.W. Robey, J.G. Tobin, L.E. Klebanoff, and D.A. Shirley, Phys. Rev. Lett. 51, 272 (1983).
7. E.L. Bullock, C.S. Fadley, P.J. Orders, Phys. Rev. B 28, 4867 (1983).
8. M. Abramowitz, I.A. Stegun, Handbook of Mathematical Functions, National Bureau of Standards, Appl. Math. Serv. 55, 1964.
9. L.I. Schiff, Quantum Mechanics, 3rd edition, McGraw-Hill, New York, 1968.
10. P.A. Lee and J.B. Pendry, Phys. Rev. B 11, 2795 (1975).
11. This is the same formula as given in Pendry, ref. 1, his Appendix A. Note that his factor  $i^{l-l'-l''}$  is equal to  $i^{-l+l'+l''}$  whenever the Gaunt integral is nonzero.
12. R. Nozawa, J. Math. Phys. 7, 1841 (1966).
13. B. Van der Pol, Physica 3, 393 (1936).
14. When the differential operator is applied to generate the addition theorem, derivatives may be taken with either  $\vec{a}$  or  $\vec{r}'$  constant, where  $\vec{a}+\vec{r}'=\vec{r}$ . Nozawa uses the physically more appealing choice of  $\vec{a}$  constant; our results follow most readily if  $\vec{r}'$  is constant for the

- purpose of the lifting operation. The equivalence of these two avenues may be proven by, for example, considering the Fourier transform derivation of the addition theorem as given by Nozawa.
15. C. Cohen-Tannoudji, B. Diu, F. Laloe, Quantum Mechanics, John Wiley and Sons, New York, 1977.
  16. B. Sinkovic, P.J. Orders, C.S. Fadley, R. Trehan, Z. Hussain, and J. Lecante, submitted to Phys. Rev. B.
  17. J.J. Barton, C.C. Bahr, Z. Hussain, S.W. Robey, L.E. Klebanoff, and D.A. Shirley, Soc. Photo-Optical Instr. Eng. 447, 82 (1984); J.J. Barton and D.A. Shirley, "A Generalized Ramsauer-Townsend Resonance in ARPEFS Oscillations," LBL-19325, to be published.
  18. J.J. Rehr, E.A. Stern, R.L. Martin, and E.R. Davidson, Phys. Rev. B 17, 560 (1978).
  19. P. Eisenberger and B. Lengeler, Phys. Rev. B 22, 3551 (1980).
  20. P.H. Citrin, P. Eisenberger, and R.C. Hewitt, Phys. Rev. Lett. 45, 1948, (1980).
  21. H.A. Bethe and R. Jackiw, Intermediate Quantum Mechanics, 2nd edition, W.A. Benjamin, Reading, MA., 1968.
  22. B.K. Teo, Proc. Intl. Conf. EXAFS and Near Edge Structure, ed. A. Bianconi, L. Incoccia, and S. Stipcich, Springer-Verlag 1983, p. 11.
  23. W.L. Schaich, Phys. Rev. B 29, 6513 (1984); J.E. Muller and W.L. Schaich, Phys. Rev. B 27, 6489 (1983).
  24. S.J. Gurman, N. Binsted, and I. Ross, J. Phys. C 17, 143 (1984).

## FIGURE CAPTIONS

- Figure 1. Scattering factor amplitude in  $\text{\AA}$  for Ni atom potential at  $k = 5\text{\AA}^{-1}$  (95 eV). Solid line is  $|f_{\text{aR}}^{00}|$ , the  $\ell=0$  spherical wave scattering factor; dashed line, plane wave limit  $2ka \gg \ell(\ell+1)$ . Right hand panel gives cartesian plots of factor magnitude versus scattering angle,  $\theta_{\text{aR}}$  in degrees; left hand panel is a polar plot with  $\theta_{\text{aR}} = 0^\circ$  running up the figure.
- Figure 2. Radial derivative scattering factor amplitude,  $|f_{\text{aR}}^{10}|$  in  $\text{\AA}$  for Ni atom potential at  $k = 5\text{\AA}^{-1}$  (95 eV). Format described in Figure 1. Note the scale of this figure is 1/20th of Figure 1.
- Figure 3. Angular derivative scattering factor amplitude  $|f_{\text{aR}}^{01}|$  times sine of the scattering angle,  $\theta_{\text{aR}}$ , in  $\text{\AA}$  for Ni potential at  $k = 5\text{\AA}^{-1}$  (95 eV). Format described in Figure 1. This scattering factor cannot contribute in near forward or near backscattering directions.
- Figure 4. Identical to Figure 1, except  $k = 10\text{\AA}^{-1}$  (381 eV). Note the improved accuracy of the plane wave limit for backscattering angles. The figure has the same scale as figure 1 to emphasize backscattering angles.
- Figure 5. Identical to Figure 2 except for  $k = 10\text{\AA}^{-1}$  (381 eV).
- Figure 6. Identical to Figure 3, except for  $k = 10\text{\AA}^{-1}$  (381 eV). Note that shift of the main peak to lower angles; its amplitude is similar to the amplitude of the main peak at  $k = 5\text{\AA}^{-1}$ , but the correction for backscattering is very much smaller now.

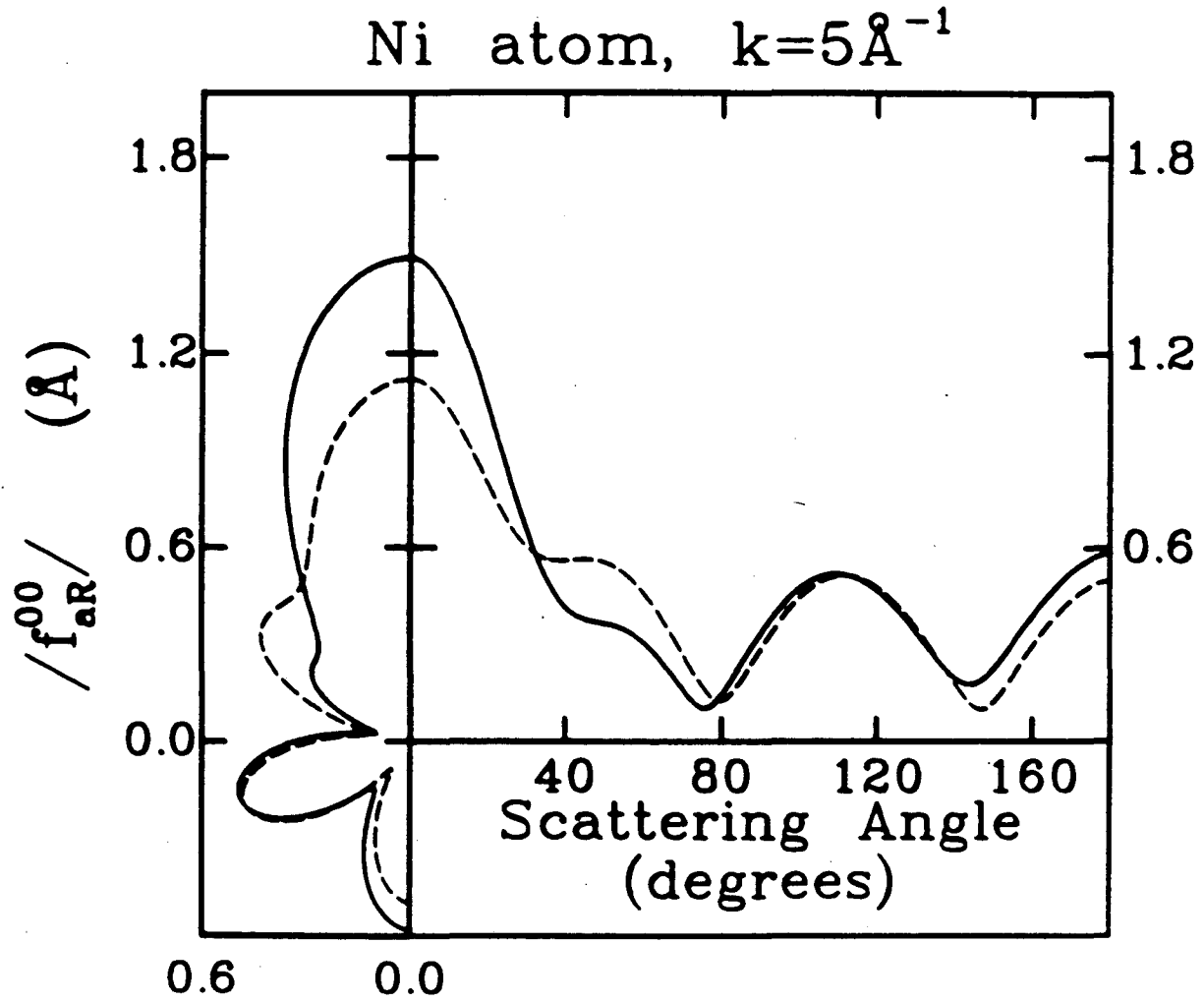
- Figure 7. Difference in phase (in radians) between spherical and plane-wave models versus scattering angle  $\theta_{aR}$  in degrees, for scattering from Ni atom potentials at  $k = 5\text{\AA}^{-1}$ .
- Figure 8. Scattering factor amplitudes in  $\text{\AA}$  versus electron wavenumber ( $\text{\AA}^{-1}$ ) for near backscattering ( $\theta_{aR} = 173^\circ$ ) from Ni atom potentials. Solid line, basic spherical scattering factor  $f_{aR}^{00}$ ; circles, plane-wave limit scattering factor  $f_{aR}$ ; triangles, radial derivative scattering factor  $f_{aR}^{10}$ . The plane-wave factor is rather close to the spherical wave  $f_{aR}^{00}$  and the other spherical wave corrections are very small at all energies; notice also that plane wave error approaches a non-zero constant.
- Figure 9. Scattering factor amplitude in  $\text{\AA}$  versus electron wavenumber ( $\text{\AA}^{-1}$ ) for forward scattering ( $\theta_{aR} = 0^\circ$ ). Solid line, basic spherical scattering factor  $f_{aR}^{00}$ ; circles, plane-wave limit scattering factor  $f_{aR}$ ; triangles, radial derivative scattering factor  $f_{aR}^{10}$ . Note the nearly constant plane-wave error; the radial derivative correction becomes almost 10 percent at low energies.
- Figure 10. Scattering factor amplitudes in  $\text{\AA}$  versus electron wavenumber ( $\text{\AA}^{-1}$ ) for scattering through  $\theta_{aR} = 127^\circ$ , the position of a Generalized Ramsauer Townsend resonance. Solid line, basic spherical wave factor  $f_{aR}^{00}$ ; circles, plane-wave limit  $f_{aR}^{\text{plane}}$ ; crosses, angular derivative  $f_{aR}^{01}$ . The radial derivative is negligible at this angle for all energies.
- Figure 11. Phase shifts for scattering from Ni. The dashed line shows the phase shift function  $\phi_j$  calculated with plane-wave

theory for  $\theta=127^\circ$ . The dotted line is the phase shift from the experimental curve. The zero crossing jump in phase occurs too high in wavenumber in the plane-wave limit. Solid lines are curved-wave calculations of the phase shift function for the indicated scattering angles.

Figure 12. Radius for acceptable results from plane wave calculations versus bond angle for  $k = 5\text{\AA}^{-1}$  (solid line) and  $k = 10\text{\AA}^{-1}$  (line with circles). The radii were selected so that all distances greater than the plotted lines have  $|f_{\text{AR}}^{\text{OO}} - f_{\text{AR}}^{\text{plane}}| < 0.06\text{\AA}$ .

Figure 13. Scattering factors for (1s) EXAFS. Solid line is  $f^{\text{iso}}$ , the curved wave scattering amplitude defined by eqn. B13. Line with circles is the plane wave limit which has a similar shape to  $f^{\text{iso}}$ . Line with triangles is  $f^{\text{an}}$ , eqn. (B13) multiplied by a factor of 50.

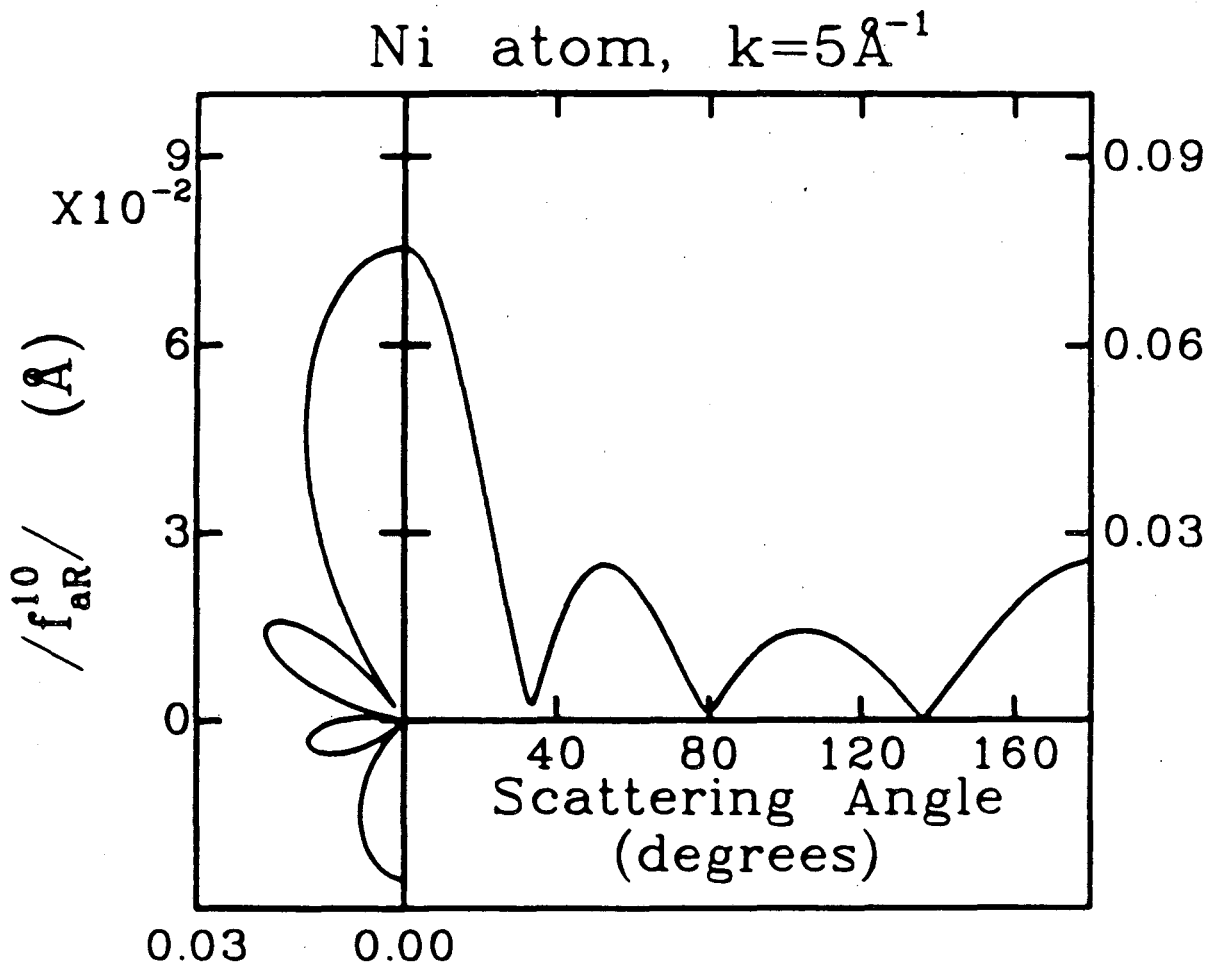
Figure 14. Schematic semiclassical orbits for an attractive potential. If the circle represents the effective radius of a screened nuclear charge, then particles with large impact parameters will sample only the weak outer region of the potential and scatter through small (forward) angles. Particles with small impact parameters orbit the strong nuclear attraction and exit at large (backscattering) angles. The connection to wave scattering is made through  $b = \ell/k$  where  $b$  is the impact parameter: large  $\ell$  partial waves contribute to forward scattering and small  $\ell$  waves dominate for backscattering.



XBL 852-1310

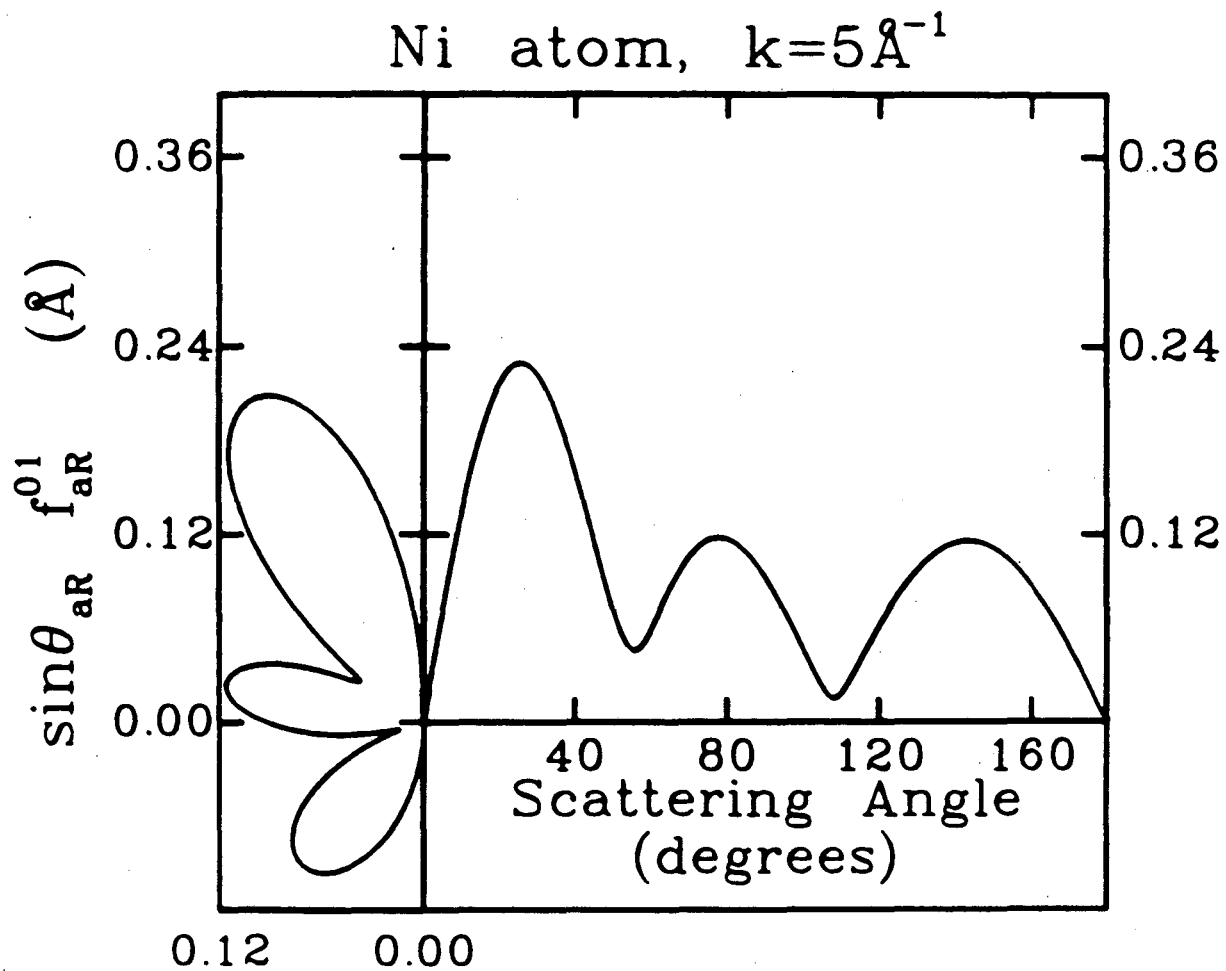
Figure 1





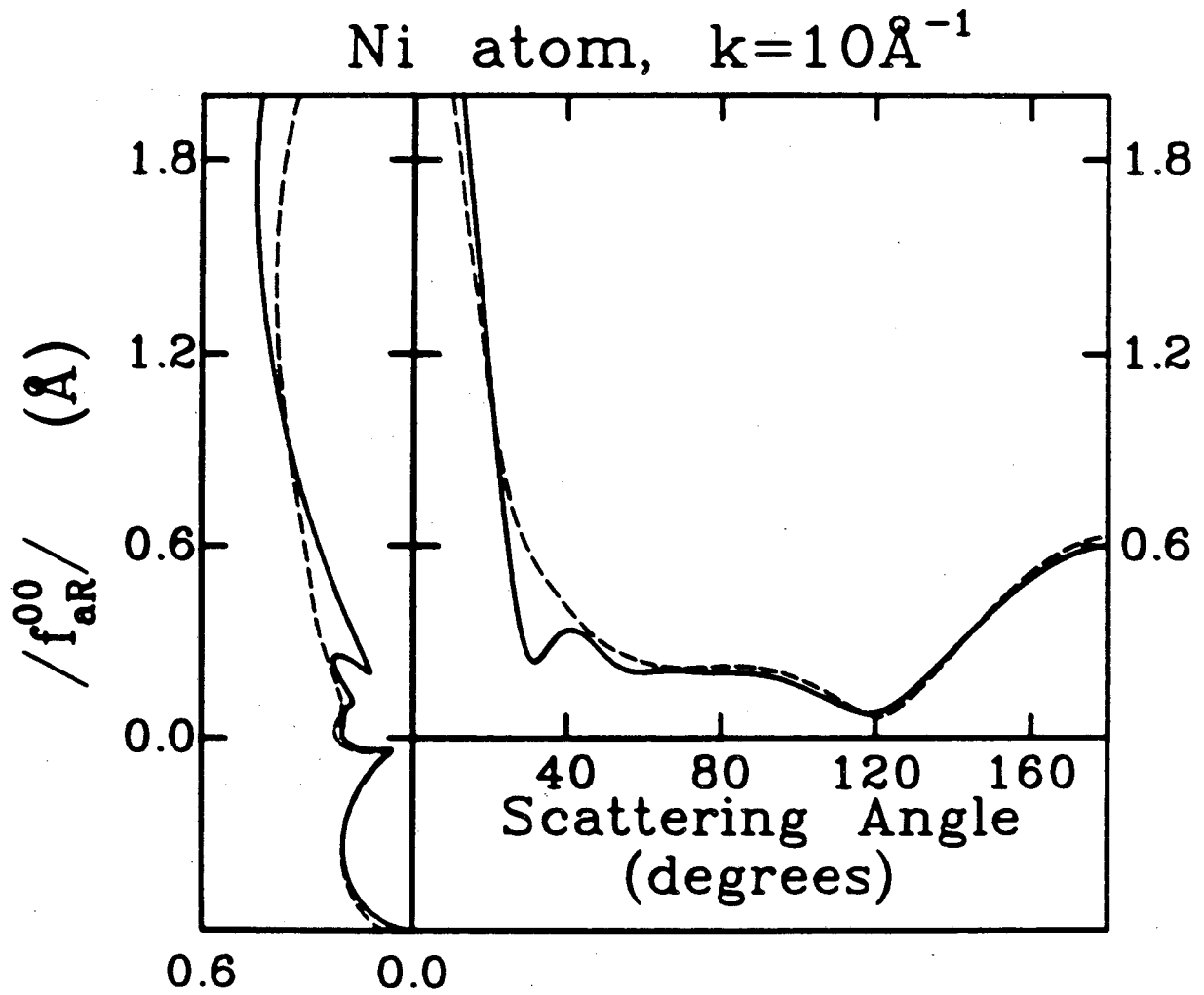
XBL 852-1311

Figure 2



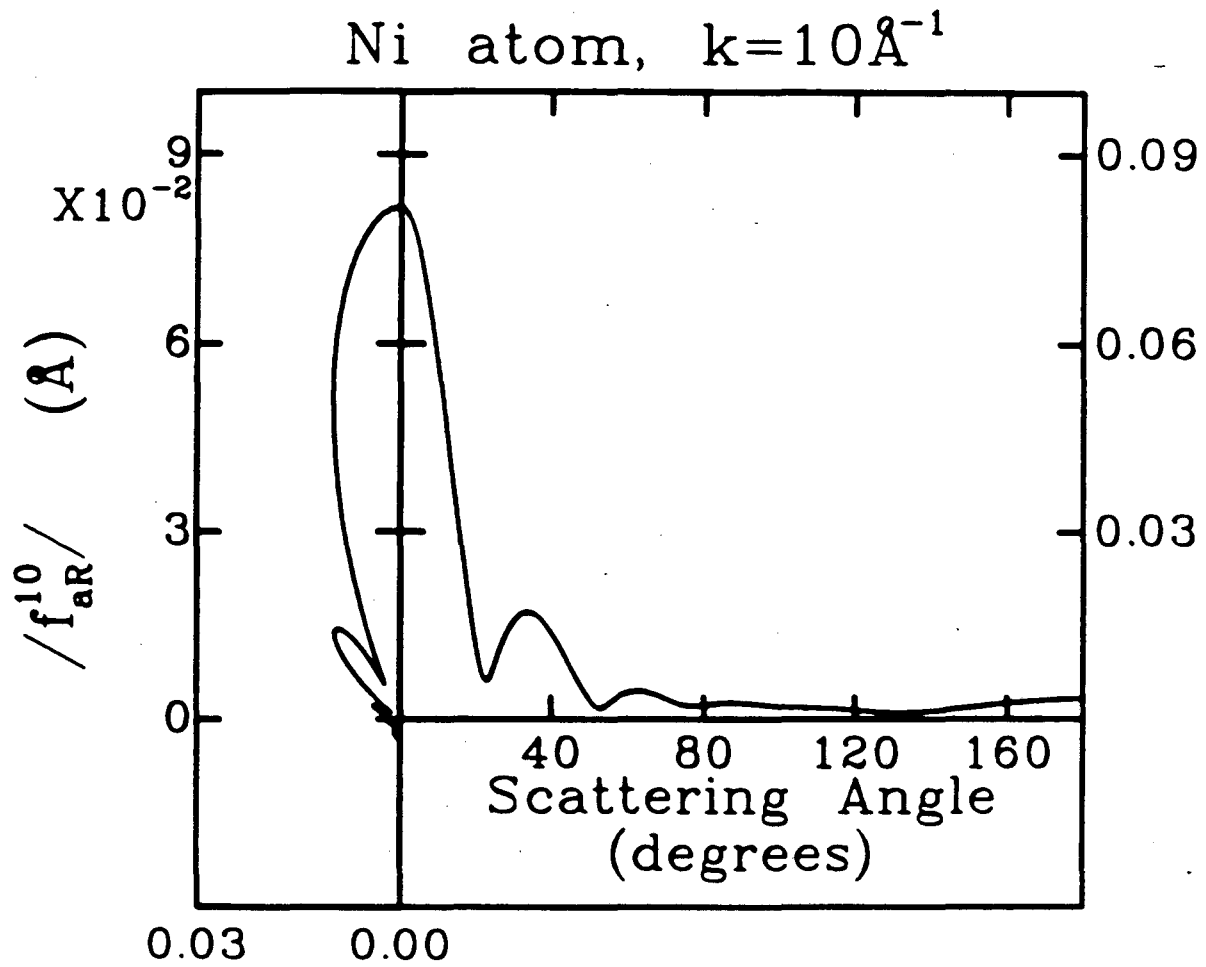
XBL 852-1312

Figure 3



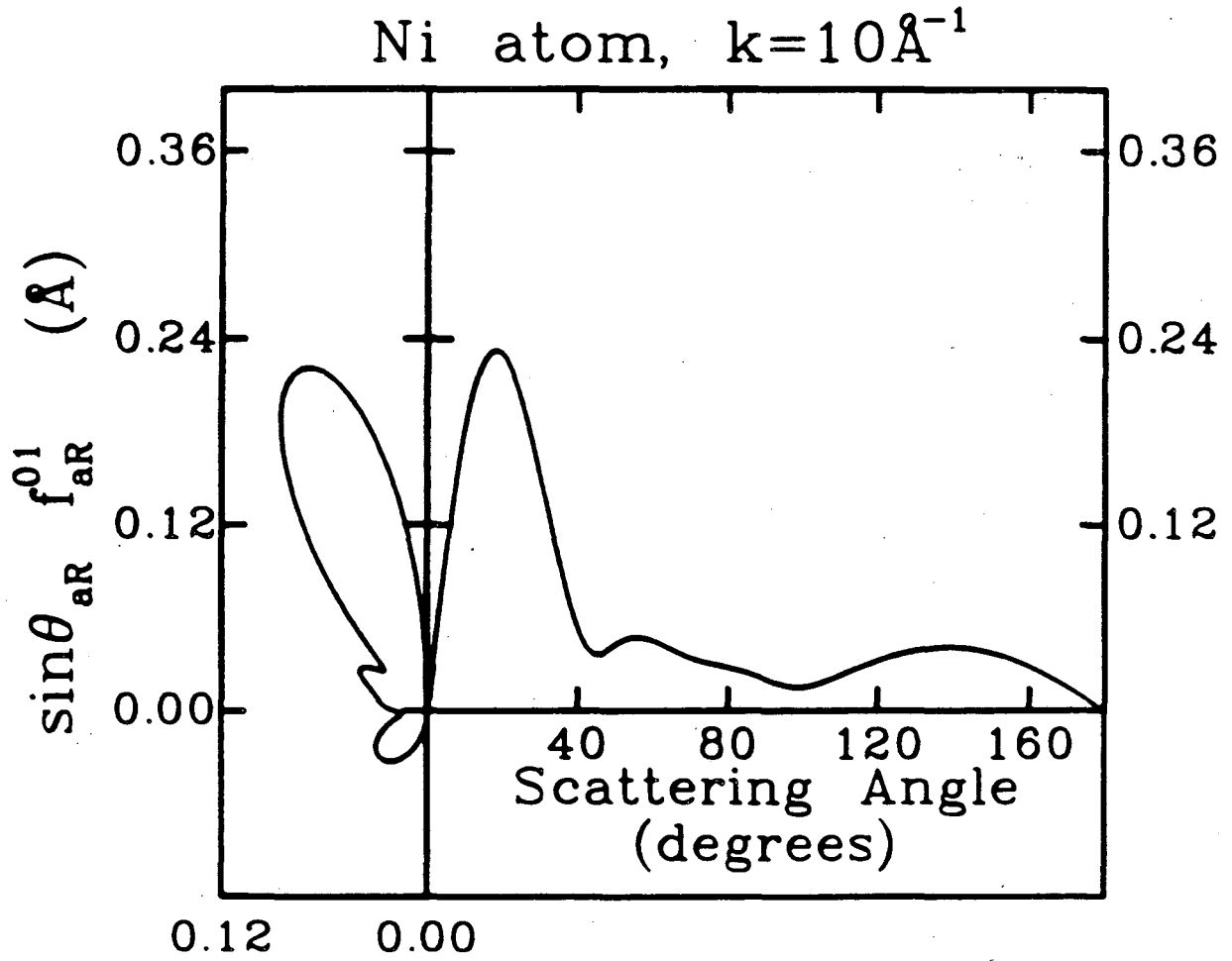
XBL 852-1313

Figure 4



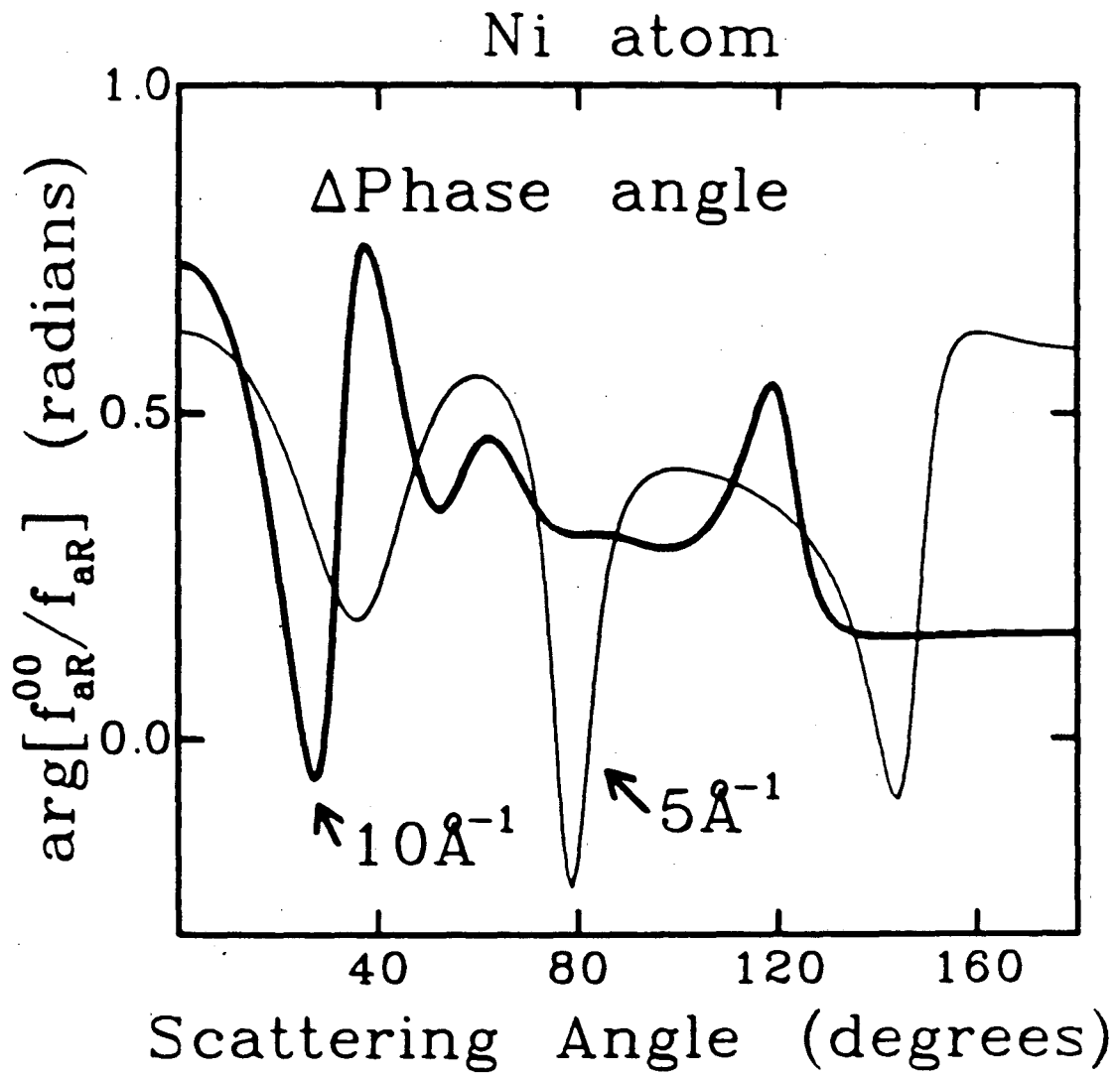
XBL 852-1314

Figure 5



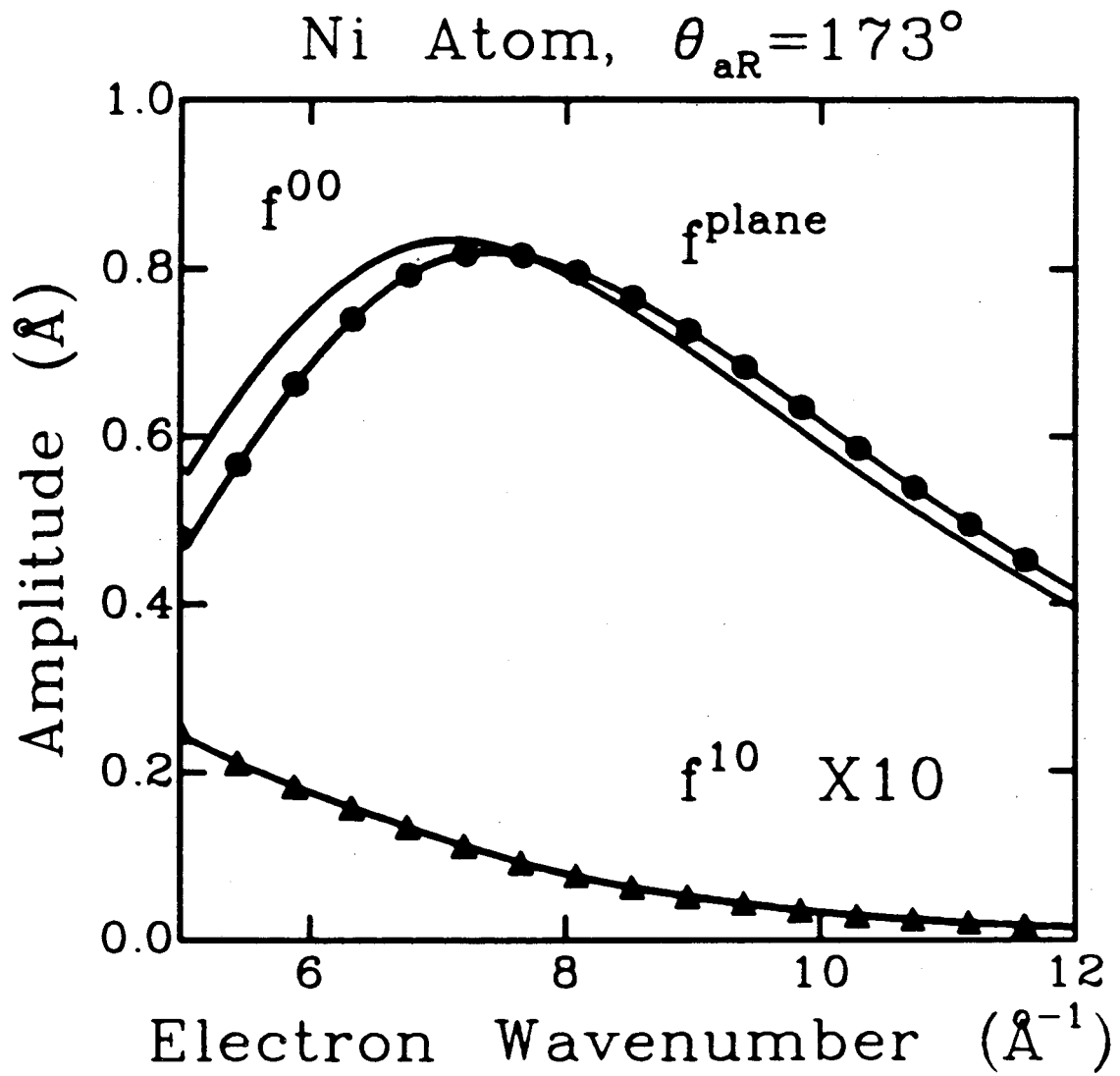
XBL 852-1315

Figure 6



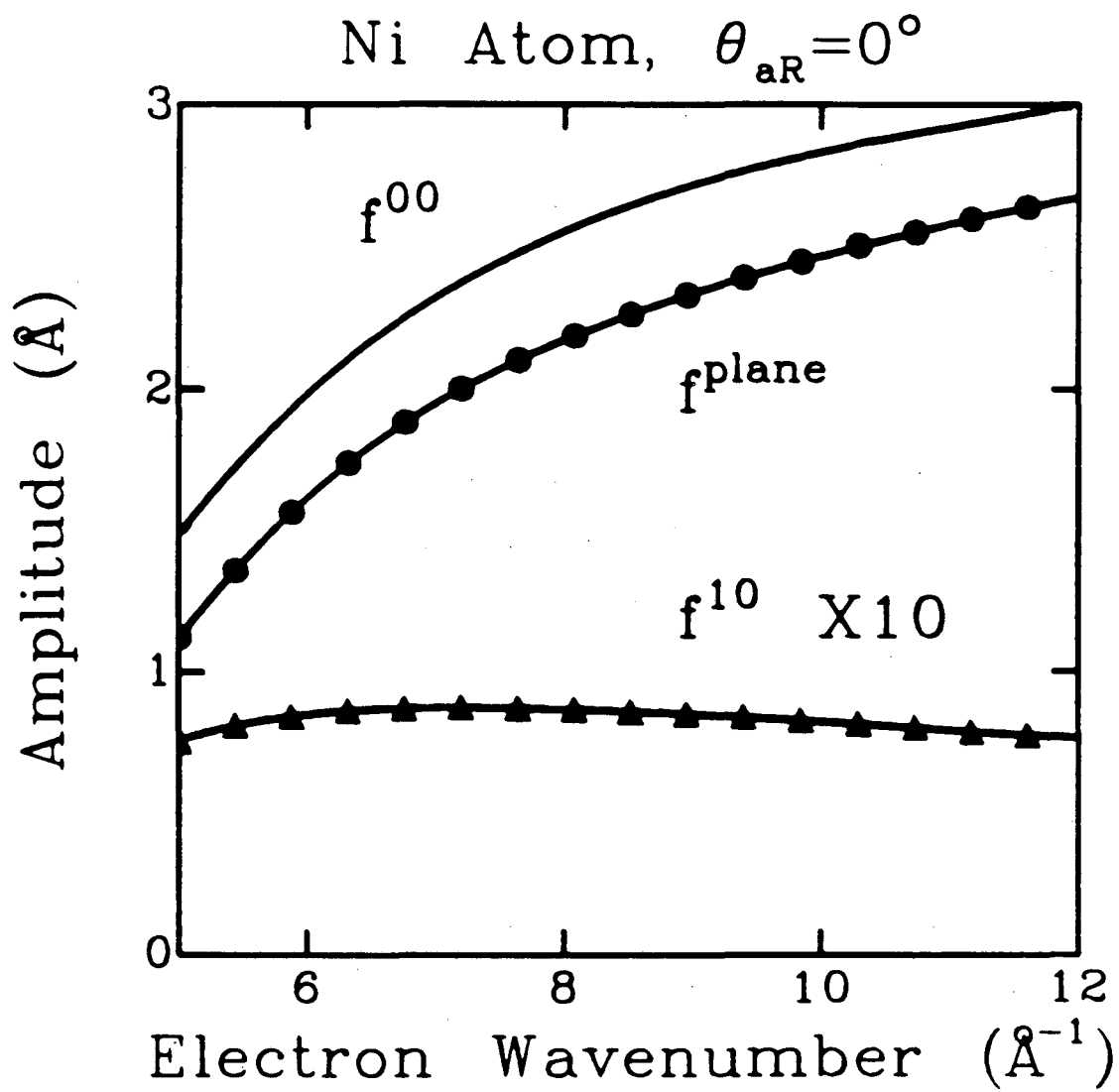
XBL 852-1316

Figure 7



XBL 852-1318

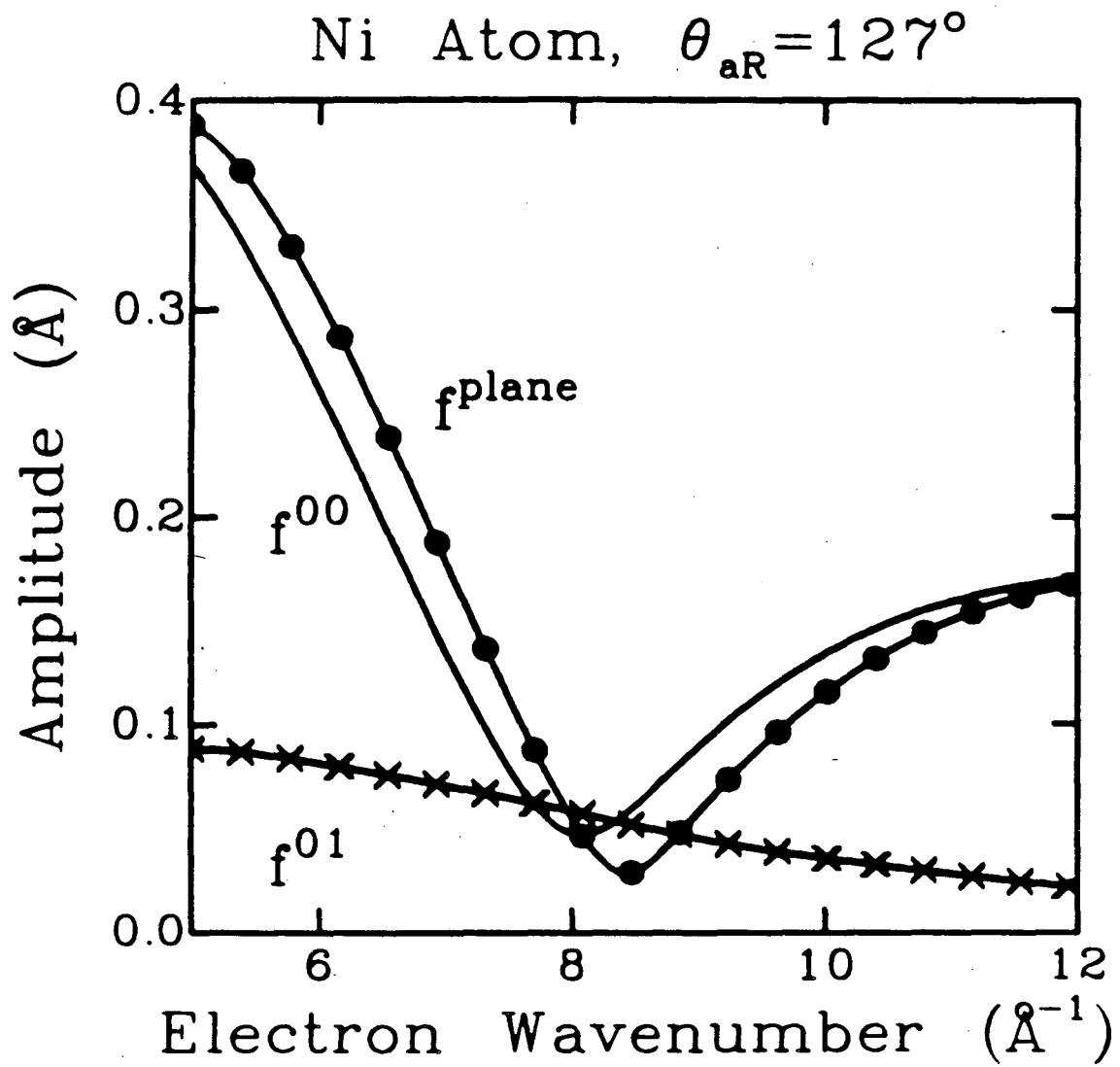
Figure 8



XBL 852-1317

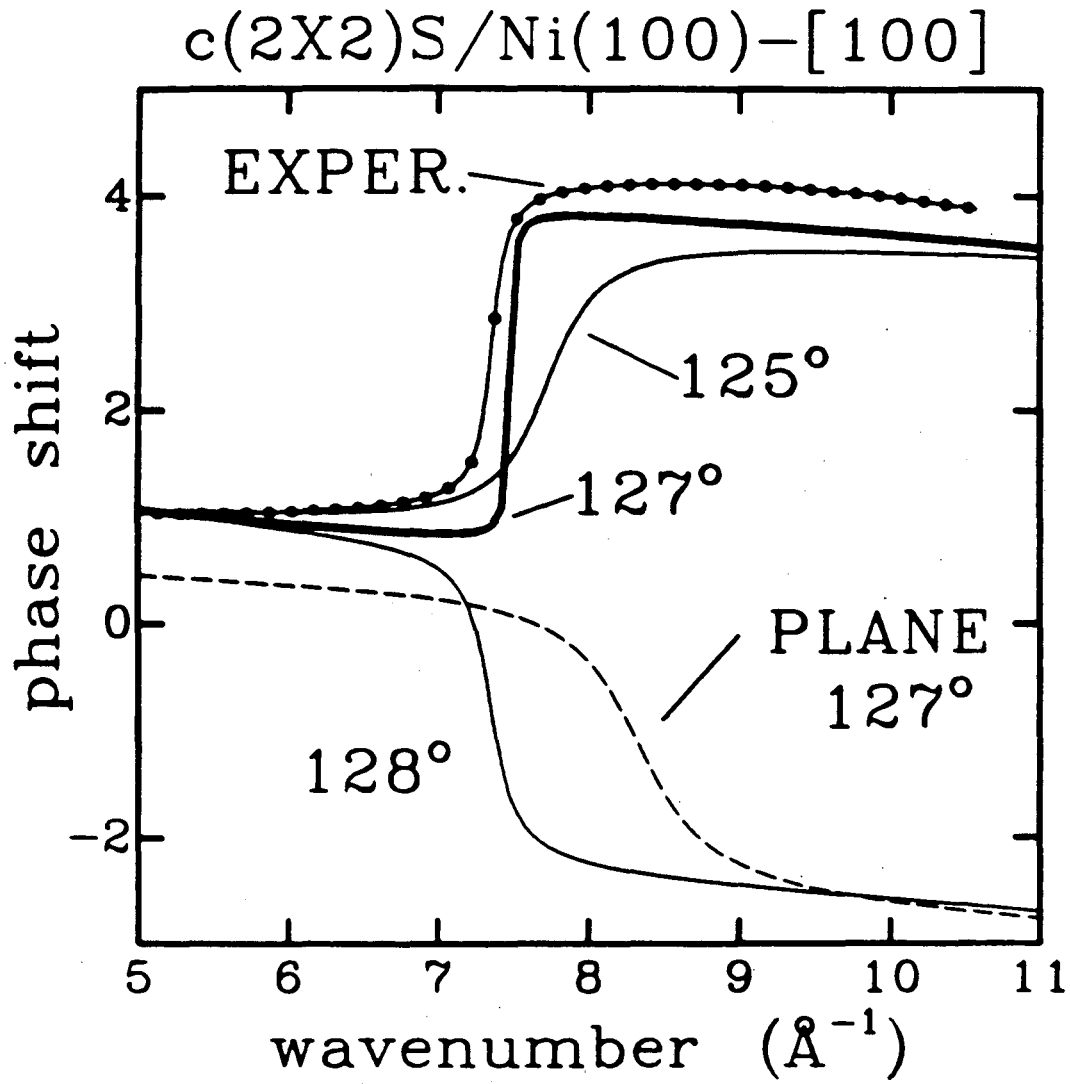
Figure 9





XBL 852-1319

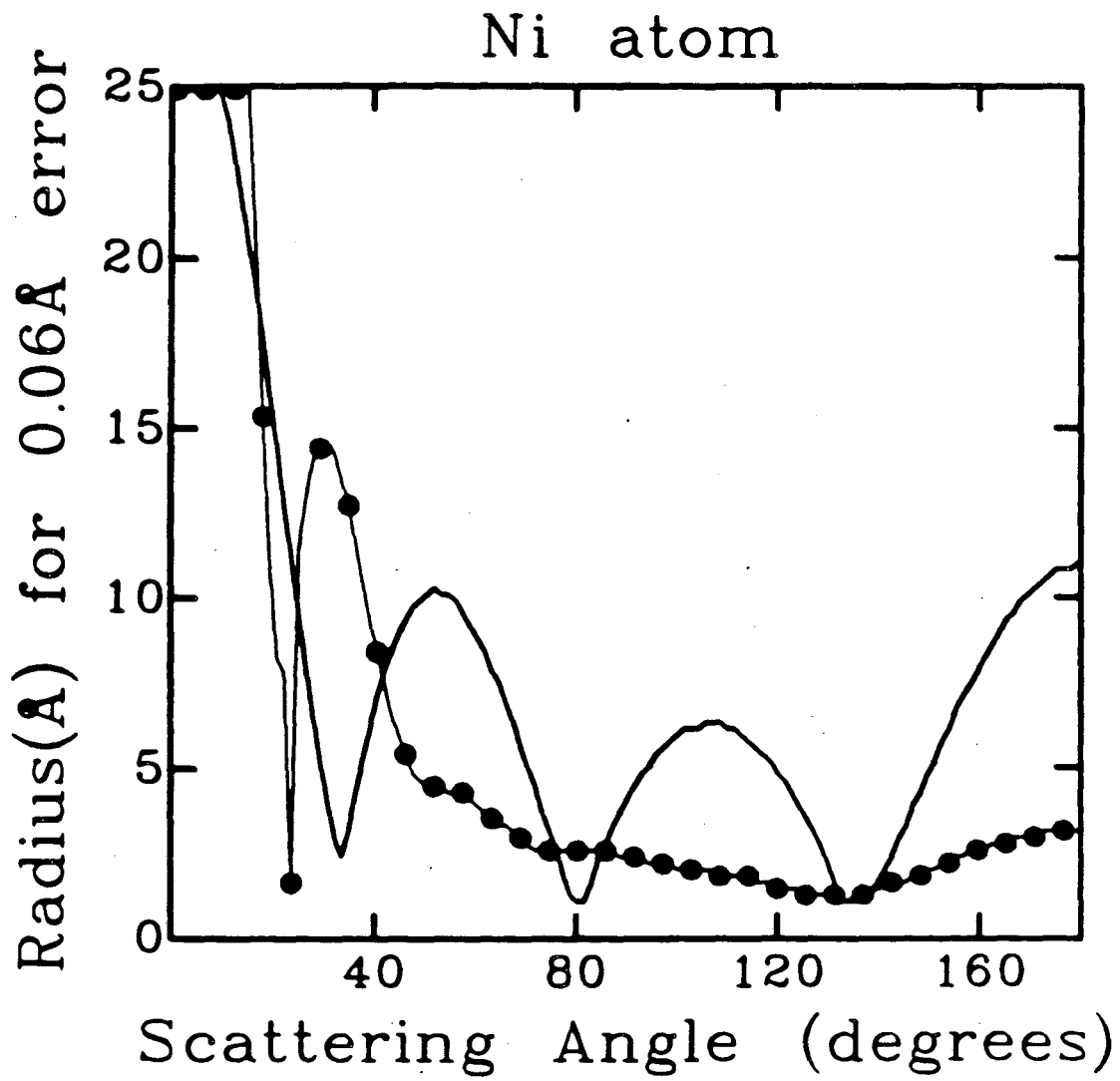
Figure 10



DK:NIS111.DUS

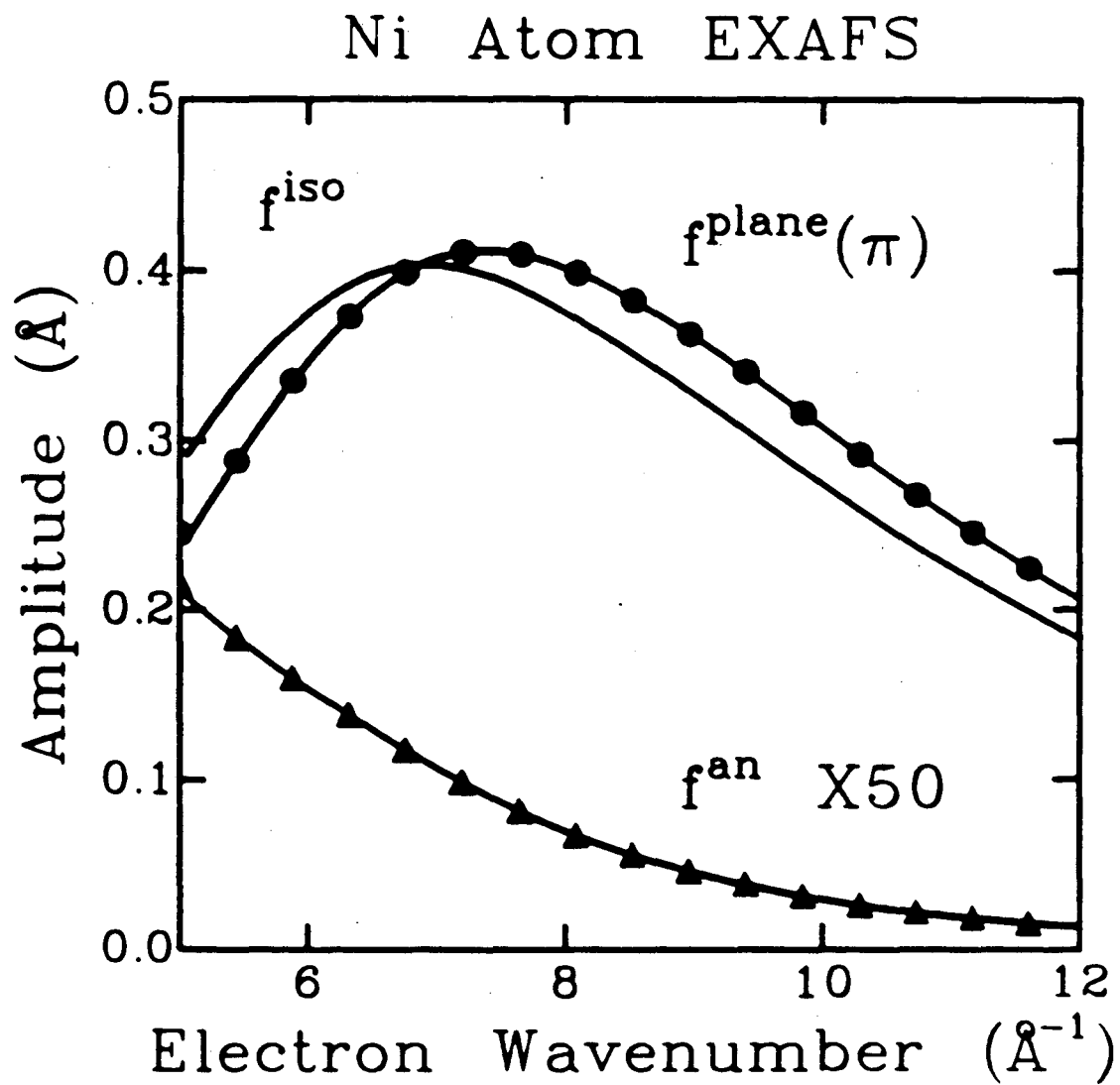
XBL 848-3548

Figure 11



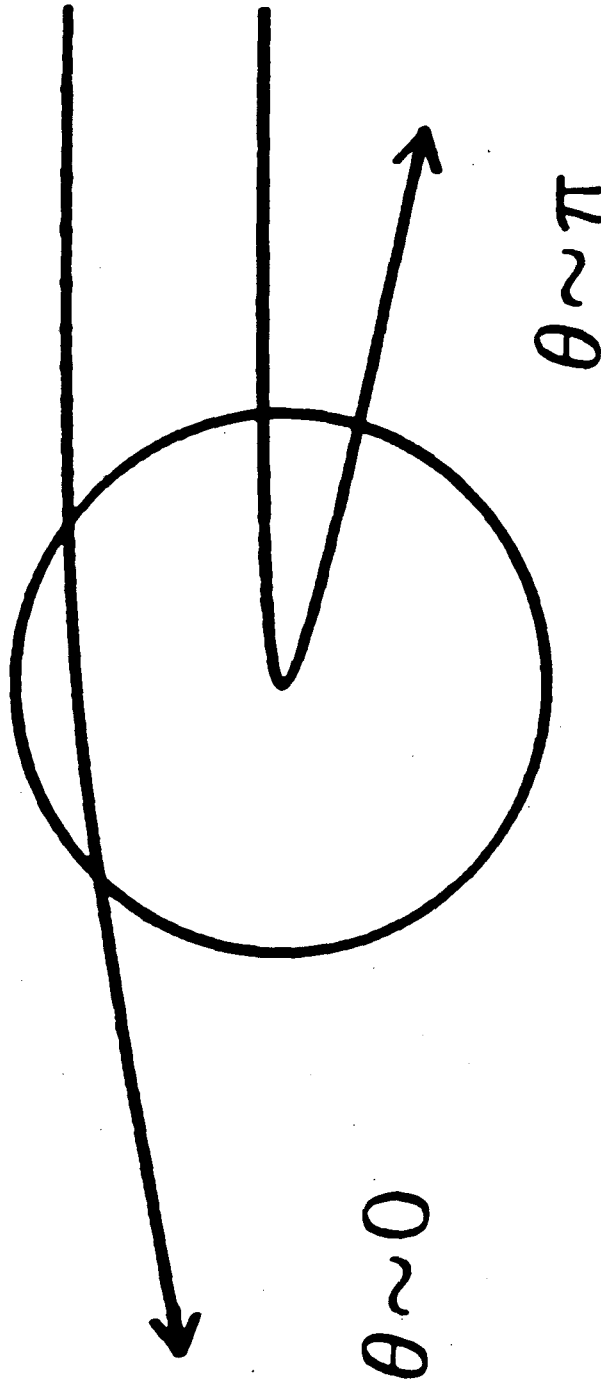
XBL 852-1320

Figure 12



XBL 852-1321

Figure 13



XBL 851-1021

Figure 14

This report was done with support from the Department of Energy. Any conclusions or opinions expressed in this report represent solely those of the author(s) and not necessarily those of The Regents of the University of California, the Lawrence Berkeley Laboratory or the Department of Energy.

Reference to a company or product name does not imply approval or recommendation of the product by the University of California or the U.S. Department of Energy to the exclusion of others that may be suitable.

TECHNICAL INFORMATION DEPARTMENT  
LAWRENCE BERKELEY LABORATORY  
UNIVERSITY OF CALIFORNIA  
BERKELEY, CALIFORNIA 94720